



Translational selenium nanoparticles boost GPx1 activation to reverse HAdV-14 virus-induced oxidative damage

Yinghua Li^{b,1}, Ting Liu^{a,1}, Ruilin Zheng^b, Jia Lai^b, Jingyao Su^b, Jiali Li^b, Bing Zhu^{b,**}, Tianfeng Chen^{a,c,*}

^a Department of Chemistry, Jinan University, China

^b Center Laboratory, Guangzhou Women and Children's Medical Center, Guangzhou Medical University, Guangzhou, China

^c Key Laboratory of Viral Pathogenesis & Infection Prevention and Control (Jinan University), Ministry of Education, China

ARTICLE INFO

Keywords:

Selenium speciation
Selenium nanoparticles
HAdV-14
Apoptosis
GPx1

ABSTRACT

Human adenovirus (HAdV) can cause severe respiratory infections in immunocompromised patients, but its clinical treatment is seriously limited by side effects of drugs such as poor efficacy, low bioavailability and severe nephrotoxicity. Trace element selenium (Se) has been found will affect the disease progression of pneumonia, but its antiviral efficacy could be improved by speciation optimization. Therefore, herein we performed *anti*-HAdV effects of different Se speciation and found that lentinan (LNT)-decorated selenium nanoparticles (SeNPs) exhibited low cytotoxicity and excellent *anti*-HAdV antiviral activity. Furthermore, SeNPs@LNT reduced the HAdV infection-induced mitochondrial damage and excessive production of reactive oxygen species (ROS). It was also involved in the repair of host cell DNA damage and inhibition of viral DNA replication. SeNPs@LNT inhibited HAdV-induced apoptosis mainly by modulating the p53/Bcl-2 apoptosis signaling pathway. *In vivo*, SeNPs@LNT replenished Se by targeting the infected site through the circulatory system and was involved in the synthesis of Glutathione peroxidase 1 (GPx1). More importantly, GPx1 played an antioxidant and immunomodulatory role in alleviating HAdV-induced inflammatory cytokine storm and alleviating adenovirus pneumonia in Se-deficient mice. Collectively, this study provides a Se speciation of SeNPs@LNT with *anti*-HAdV activity, and demonstrate that SeNPs@LNT is a promising pharmaceutical candidate for the treatment of HAdV.

1. Introduction

Severe adenovirus pneumonia is viral pneumonia and one of the most serious types of pediatric pneumonia. Human Adenovirus (HAdV) is an enveloped double-stranded DNA virus that can cause respiratory tract infection in children [1]. Adenovirus Type 14 (HAdV-14) was originally isolated from the Dutch army in 1955 and identified as a pathogen causing acute respiratory disease. HAdV-14 belongs to the B subgenus of HAdV, which primarily causes respiratory tract infections [2]. Compared with general pathogens that only infect the upper respiratory tract, HAdV-14 that can infect the lower respiratory tract have a higher rate of severe pneumonia [3]. HAdV-14 is characterized by its rapid onset, rapid transmission, and high mortality rate. It is also the primary type responsible for mutated strains. HAdV-14 has caused

severe outbreaks of respiratory disease and even deaths in both China and the United States, and HAdV-55 is a novel virus composed of a recombination of the HAdV-11 and HAdV-14 genes, which make up the majority of the HAdV-14 genome [4–6]. Once adenovirus pneumonia develops into severe pneumonia characterized by acute respiratory distress syndrome (Ards), the patient may suffer severe lung injury or even die from multiple organ dysfunction syndrome. In patients with severe pneumonia caused by adenovirus infection, in addition to the respiratory system, other systems are often involved, such as the nervous system and digestive system. Severe adenovirus pneumonia often leads to serious complications such as nerve damage, liver damage, myocardial damage, and shock [7]. The pathogenesis of HAdV-14 infection is still not clear and there is no specific drug against HAdV-14 infection, the broad-spectrum antiviral and immunotherapy strategies are still

Peer review under responsibility of KeAi Communications Co., Ltd.

* Corresponding author.

** Corresponding author.

E-mail addresses: zhubing@gzhmu.edu.cn (B. Zhu), tchentf@jnu.edu.cn (T. Chen).

¹ These authors contributed equally to this work.

<https://doi.org/10.1016/j.bioactmat.2024.04.034>

Received 3 March 2024; Received in revised form 18 April 2024; Accepted 29 April 2024

2452-199X/© 2024 The Authors. Publishing services by Elsevier B.V. on behalf of KeAi Communications Co. Ltd. This is an open access article under the CC BY-NC-ND license (<http://creativecommons.org/licenses/by-nc-nd/4.0/>).

adopted in the clinical treatment of HAdV-14 infection. Anti-adenoviral drugs have specific antiviral effects against pathogens, which means they can solve problems at the source [8,9]. Thus, they have important clinical significance for inhibiting the development of diseases.

The Adenovirus infection antiviral drug can be divided into two main categories according to the different antiviral mechanisms, including DNA polymerase inhibitors and broad-spectrum antiviral drugs [10,11]. Among them, DNA polymerase inhibitors mainly inhibit DNA polymerase and thus affect the production of viral DNA [12], and broad-spectrum antiviral drugs can inhibit viral DNA replication and RNA transcription and they are effective for a variety of viral infections [13]. As a non-enveloped double-stranded DNA virus, when HAdV infects the host cells, the DNA replication process would be carried out in the nucleus. Thus, DNA polymerase inhibitors are the common choice for specific anti-adenoviral drugs in clinical treatment. Cidofovir is a nucleotide analog that can inhibit the HAdV DNA polymerase after being converted into the bisphosphate form in the cells, in order to terminate the viral DNA chain [14]. At present, cidofovir is a clinically recommended drug for the treatment of adenovirus. However, the use of cidofovir has certain limitations [15]. For example, the application of cidofovir in the early stage of HAdV infection has a higher effective rate. However, the early clinical manifestations of children with adenovirus pneumonia have no obvious specificity, and it is difficult to distinguish them from common respiratory pathogen infections only by physical signs and inflammatory indicators which increases the difficulty of early clinical identification and diagnosis. More importantly, cidofovir has low bioavailability, low cell penetration, and severe nephrotoxicity. Due to the lack of medication standards, treatment may cause irreversible sequelae in children [16]. These factors greatly reduce the clinical effective treatment of HAdV infection, and miss the best time for treatment.

Lentinan (LNT) is involved in a variety of anti-pathogen and immune regulation activities, such as antioxidant, immunomodulatory, anti-tumor, antiviral and antibacterial functions. In order to optimize the Bioavailability of LNT and exert its excellent biological activity, the structure modification of LNT and nanoparticles is the research hotspot [17,18]. In the previous research of Ren G et al., the LNT was selenized by the $\text{HNO}_3\text{-Na}_2\text{SeO}_3$ method to convert the LNT-modified selenium nanoparticles (SeNPs). The surface structure and main elements of polysaccharides and SeNPs have undergone great changes [19]. LNT effectively disperses and stabilizes SeNPs of different sizes through the structure of Se–O–C, O–Se–O, and Se=O to improve the bioavailability and bioactivity of Se element while retaining the excellent biological activity of LNT [20]. In the human body, Se is one of the essential micronutrients, and it is related to many metabolic pathways, among which the most familiar are the regulation of antioxidant function and immune function. Meanwhile, the infection of respiratory viruses such as HAdV-14 has a certain correlation with the reduction of Se content in the body [21]. As a special form of Se, SeNPs have lower toxicity and higher biocompatibility than inorganic Se and organic Se, and retains the antioxidant and immunomodulatory functions of Se [22]. More importantly, SeNPs is added not only as a carrier to drug synthesis but also because of the redox regulation of Se. According to previous studies, SeNPs have good applications in cell models and animal models of many diseases, including various cancers and infectious diseases [23,24]. In the chemotherapy of tumor, SeNPs can not only act as the carrier of drug delivery, but also participate in the regulation of protein and DNA biosynthesis and the activity of protein kinase C, which can inhibit the proliferation of cancer cells [25]. An increasing number of research also suggests that SeNPs could be used as a potential immunotherapy. SeNPs interact directly with innate immune cells such as macrophages, dendritic cell, and natural killer cell, to regulate the activation of anti-cancer molecular signaling pathway, cell polarization, activation of cytokines, and then influence the innate immune response. In addition, SeNPs can promote T cell proliferation, differentiation, secretion, receptor expression and cytotoxicity, and then regulate the adaptive immunity.

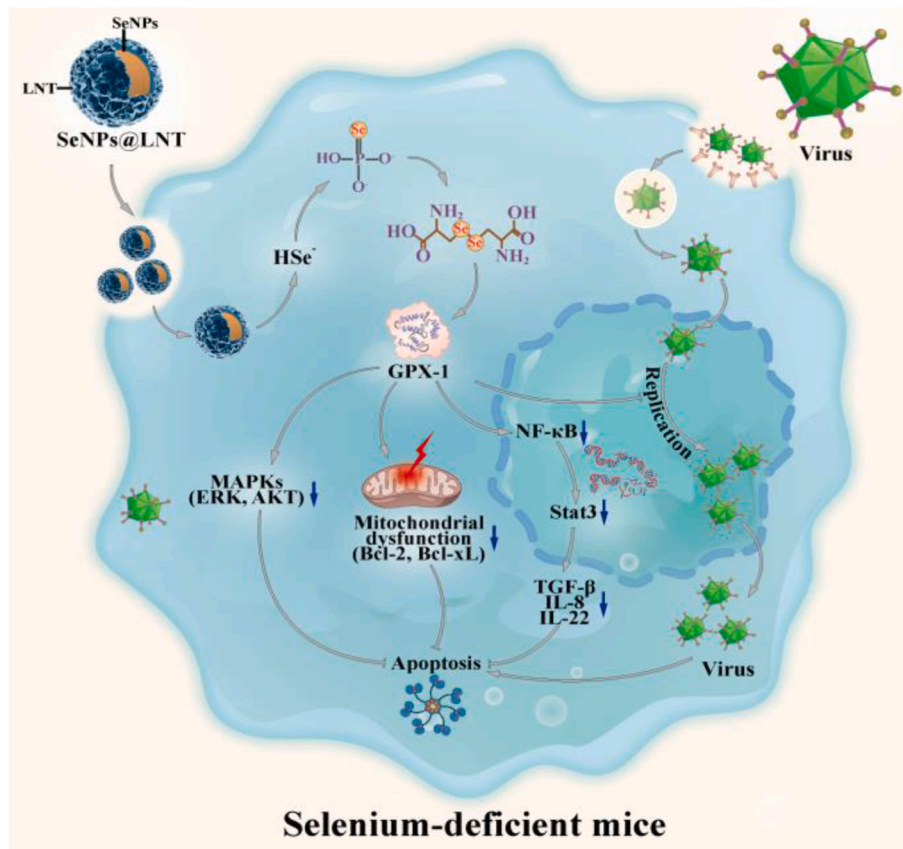
Recent studies on SeNPs as adjuvant for viral vaccine have shown that SeNPs can modulate the expression of GPxs in immune cells, enhance immunity and modulate redox activity, effectively improve its function and responsiveness to vaccination [26]. SeNPs have potential in the development of anti-cancer, anti-infection and anti-inflammatory therapeutic strategies [27,28]. Among them, SeNPs works mainly by converting to selenoproteins *in vivo* [29]. Glutathione peroxidase (GPx), as an important selenoprotein in the body, plays an important role in antioxidant defense [30]. At the same time, selenoproteins have a regulatory effect on immune cells in inflammatory environments and the immune homeostasis changes induced by inflammatory factors produced by them [31]. Previous studies have shown that in the case of respiratory virus infection, the Se content and GPx in the body tend to decrease, indicating that the metabolism of Se is closely related to virus infection [32–34]. While, our prior investigation revealed that SeNPs lacking surface decoration exhibited significant aggregation and precipitation, rendering them unsuitable for the intended application. In contrast, surface-decorated SeNPs were observed to maintain monodispersed spherical morphology in aqueous media, and exhibited sustained stability [35]. Consequently, solitary SeNPs treatment was omitted from the present study. Furthermore, our observations indicated that LNT-functionalized SeNPs exhibited favorable attributes, including low cytotoxicity, efficient cellular uptake, and sustained stability [36]. Research from B. Xie et al. suggests that, SeNPs@LNT can increase the Se content and selenoprotein expression in the skin, reduce mast cell activation and inflammatory cell infiltration, and thus demonstrate effective therapeutic effects in the study of allergic dermatitis [37]. Therefore, SeNPs@LNT may exhibit its antioxidant capacity and immune regulation by enhancing the activity of selenoprotein.

In this study, we synthesized SeNPs@LNT, which exhibited synergistic effects and showed excellent antioxidant responses and antiviral abilities, for the specific treatment of HAdV-14 (Scheme 1). SeNPs@LNT inhibits HAdV-14-induced apoptosis by modulating p53/Bcl-2 apoptosis signaling pathway. Meanwhile, SeNPs@LNT alleviated the damage of inflammatory cytokine storm by inhibiting the NF κ B signal pathway in the lung of Se-deficient mice infected with HAdV-14. We hypothesized that SeNPs@LNT exerts its antioxidant activity by regulating the conversion of Se elements into selenoprotein, which enhances GPx1 level and increases Se content at the infection site to against HAdV-14. This study provides a Se-containing drug with *anti*-HAdV-14 activity and low cytotoxicity, which has the potential to fill the gap of adenovirus-specific therapeutic drugs.

2. Materials and methods

2.1. Materials

A549 cells, derived from ATCC (USA), were subcultured in laboratory. HAdV-14 were isolated from sputum samples of patients in the central laboratory of Guangzhou Women and Children Medical Center affiliated to Guangzhou Medical University and were adaptively subcultured in A549 cells. The fetal bovine serum (FBS) from Thermo Fisher Science (USA) and DMEM containing 4.5 g/L glucose from Gibco (USA) were used as culture medium components. The penicillin/streptomycin combination antibiotics were purchased from Gibco (USA). SeNPs@LNT was generously provided by the School of Chemistry, Jinan University. Fluorescent probe reagents include JC-1 detection kit for mitochondrial membrane potential, Annexin-V apoptosis detection kit and one-step *in situ* end labeling apoptosis detection kit provided by Beyotime (China). Chemiluminescence reagents include Caspase-3 activity detection kit and enhanced cell counting kit-8 (CCK-8) purchased from Beyotime (China). Fluorescent dyes include Lyso-Tracker, DAPI and 2', 7'-dichlorofluorescein (DCF) -diacetate purchased from Sigma-Aldrich (USA). Antibodies of *p*-ATM (Ser1981), *p*-ATR (Ser428), Erk1/2, Bcl-xL, Bcl-2, Bad, T-PARP, c-PARP (Asp214), T-mTOR, *p*-mTOR (Ser2448), RIP3, β -actin, T-p38, T-p53, *p*-JNK (Thr183/Tyr185), T-JNK,



Scheme 1. Schematic diagram of SeNPs@LNT designed for the treatment of adenovirus pneumonia caused by HAdV-14 infection.

T-Caspase-3, T-Akt, and *p*-Akt (Ser473) were offered by Cell Signaling Technology (USA). The Mouse GPx1 (Glutathione Peroxidase 1) ELISA Kit (MOES01393, Reagent Genie, Ireland) and the Mouse Thioredoxin Reductase 1/TXNRD-1 ELISA Kit (MOFI01171, Reagent Genie, Ireland) were purchased from Reagent Genie (Ireland). Mice as *in vivo* animal models were obtained from Guangdong Provincial Medical Laboratory Animal Center (China). The Se-deficiency mouse model was constructed and validated by Jinan University for use in experiments. The procedures of all animal experiments were performed in accordance with the guidelines of the Guangdong Medical Laboratory Animal Center. Aimplex Cytokine Detection Kit was provided by QuantoBio (Beijing, China).

2.2. Synthesis of SeNPs@LNT

According to the previous study by Song Z et al., under low-speed stirring, 2 mL LNT solution in the concentration of 1 mg/mL was filtered through a MCE membrane filter with 0.22 μm at room temperature. The LNT solution obtained from the previous step was mixed with 2 mL Na_2SeO_3 (10 mM). After that, the mixture was added drop by drop to 2 mL of 40 mM Vc solution and reconstituted with Milli-Q water constant volume to 10 mL. The mixture was stirred for 10 h, then it was dialyzed with Milli-Q water for 24 h, unreacted LNT, Na_2SeO_3 and Vc could be eliminated. The final compound nanoparticles were named SeNPs@LNT, and the storage temperature was 4 $^\circ\text{C}$. The operations in this experiment were conducted under aseptic conditions [38].

2.3. Characterization of SeNPs@LNT

SeNPs@LNT was provided by college of chemistry and materials science, Jinan University, Guangzhou, China. ICP-MS was used to determine the concentration of Se in SeNPs@LNT. The hydrodynamic

size and the charge on the surface of synthesized LNT-SeNPs were determined by Zetasizer Nano ZS particle analyzer (Malvern Instruments Limited, UK). TEM images of SeNPs@LNT were photographed by transmission electron microscope (TEM, Hitachi H-7650, 80 kV, Japan). As well as the X-ray photoelectron spectroscopy (XPS, Thermo Scientific ESCALAB 250, UK) was used to characterize the chemical structure of SeNPs@LNT [38].

2.4. Detection of cell viability

CCK-8 assay was used to detect the activity of A549 cells to reflect the cytotoxicity of SeNPs@LNT [39]. The TCID_{50} virulence of HAdV-14 fluid was detected by Reed-Mutch two-layer method, and the titer of HAdV-14 was listed in [Supplementary Table 1](#). A549 cells were cultured in 96-well flat-bottomed cell culture plate at the density of 8×10^4 cells/mL in the condition of 37 $^\circ\text{C}$ and 5 % CO_2 . When the density of A549 cells accounted for 80 % of the bottom area of the culture bottle, 100 $\text{TCID}_{50}/\text{mL}$ HAdV-14 was used to infect the cells. The virus was co-incubated with cells at 37 $^\circ\text{C}$ and 5 % CO_2 for 2 h, and A549 cells were washed with PBS for three times to remove the uninternalized virus. SeNPs@LNT was stored in the concentration of 2.5 mM, and SeNPs@LNT was diluted with DMEM according to the concentration range of 1, 2, 4, 8, 16 μM . SeNPs@LNT was co-incubated with A549 cells for 48 h. CCK-8 reagent and DMEM were mixed at 1:10 to form the detection working solution, which was incubated with cells of different groups for about 1 h. The absorbance was measured at 450 nm after incubation.

2.5. Antiviral efficiency monitoring

RAD14EGFP, a kind of HAdV-14 with inserted eGFP gene could replicate and express viral nucleic acid while expressing eGFP after

infecting A549 cells [40]. The titer of rAD14 EGFP was listed in [Supplementary Table 2](#). As mentioned above, A549 cells were infected with rAD14EGFP with virulence 100 TCID₅₀/mL. The infected A549 cells were treated with SeNPs@LNT with a concentration gradient of 1, 2, 4, 8 μM. Fluorescence microscope (Leica, Germany) and fluorescence microplate reader (Thermo Fisher Science, USA) were used to qualitatively and quantitatively observe the specific fluorescence of HAdV-14-eGFP in infected A549 cells.

2.6. Post-exposure antiviral activity of the progeny virus

To visually confirm the viral load of HAdV-14 in A549 cells, rAD14 EGFP expressing green fluorescence was used for this experiment. Preliminary experiments were set up as virus group and SeNPs@LNT treatment group. A549 cells were plated at a density of 8×10^4 cells/mL in the 6 cm dishes. After the cells had grown to 80 %, rAD14 EGFP with virulence of 100 TCID₅₀/mL was added, and the uninternalized virus was removed after incubation at 37 °C and 5 % CO₂ for 2 h. The SeNPs@LNT treatment group was treated with SeNPs@LNT for 48 h, and the virus group had no treatment. After culturing for 48 h at 37 °C and 5 % CO₂, the suspension liquid of each group was collected for TCID₅₀ determination, and the virulence of progeny viruses after SeNPs@LNT treatment was determined. The inhibitory effect of SeNPs@LNT on progeny virus production was confirmed by observing the changes of green fluorescence intensity in the infected cells.

2.7. Detection of viral load of HAdV-14 in A549 cells and culture supernatant

Culture supernatant from different treatment groups was collected, and the remaining culture supernatant was discarded. After A549 cells were washed with PBS, Trizol (#254712, Invitrogen, Thermo Fisher Scientific, USA) was added to lyse cells for DNA extraction. The specific primers used to detect HAdV-14 were as follow: HAdV-14 forward primer, 5'-CAGCAGTCTATGCCAACAG-3', and HAdV-14 reverse primer, 5'-GCTTGGTCTCCATTTAACTGAATC-3'. The specific primers used to detect RPL-18 were as follow: RPL-18 forward primer, 5'-CCTGGATACCGCAGCTAGGA-3', and RPL-18 reverse primer, 5'-GCGGCGCAATACGAATGCCCC3', which were used as normalization controls for HAdV-14 gene of A549 cells in different groups. The reagent for qPCR quantification was SYBR Green qPCR SuperMix (Invitrogen, Thermo Fisher Scientific, USA). The qPCR reaction system was: 95 °C for 5 min (1 cycle); 94 °C for 1 min, 52 °C for 45 s, 72 °C for 45 s (35 cycles); the amplification step ended at 72 °C for 7 min. The qPCR was detected by ABI PRISM® 7500 Sequence Detection System (Thermo Fisher Scientific, USA).

2.8. Infection process of HAdV-14 in A549 cells

rAD14EGFP was a HAdV-14 with an inserted eGFP gene. HAdV-14 invaded A549 cells by adsorbing on the surface of cytomembrane and interacting with the specific receptors such as CAR and αV-integrin receptor. The eGFP-labeled HAdV-14 replicated and proliferated after entering the cells, expressing eGFP to emit green fluorescence. The green fluorescence from rAD14 EGFP was used to label the location of the viral particles in A549 cells. The red fluorescence emitted by the Lyso-tracker was used to label lysosomes, and the blue fluorescent DAPI was applied to label the nuclei. The changes of cell pathological change (CPE) and fluorescence morphology of A549 cells were continuously monitored by fluorescence microscopy, and then the position of HAdV-14 in A549 cells were recorded from 0 to 30 h.

2.9. Caspase-3 activity detection

The structural proteins of A549 cells were lysed with lysis buffer and purified by centrifugation to obtain the functional proteins. The enzyme

activity of caspase-3 in purified cell lysates was detected by spectrophotometry. Caspase-3 could bind to the substrates and catalyze Ac-DEVD-pNA (acetyl-Asp-Glu-Val-Asp *p*-nitroanilide) into pNA (*p*-nitroaniline), which was yellow. Therefore, the activity of caspase-3 was detected by measuring the absorbance near 405 nm [41].

2.10. TUNEL-DAPI co-staining assay

Apoptosis could activate several DNA endonucleases, which caused the damage of genomic DNA. In order to detect the DNA status of the cell nucleus, DAPI was used to locate the position of the nucleus in the experiment. FITC-labeled dUTP was used to detect the fragmented DNA to determine the DNA damage of A549 cells. Changes in FITC fluorescence representing fragmented DNA in the nucleus of A549 cells were observed by the fluorescence microscope [42].

2.11. Detection of phosphatidylserine transformation by flow cytometry

In the early stage of apoptosis, the membrane surface of the cells would turn over and the FITC-labeled Annexin V could specifically bind to phosphatidylserine. The necrotic cells and the late apoptotic cells might lose the integrity of the cell membrane, and propidium iodide (PI) could directly stain the DNA in the nucleus [43]. After treatment with SeNPs@LNT, the cells in different groups were stained with Annexin V-FITC and PI for 20 min. The fluorescence changes of A549 cells were observed by fluorescence microscope, and the proportion of apoptotic and necrotic cells were detected by BD FACSCanto II flow cytometer (BD Biosciences).

2.12. Change of mitochondrial membrane potential ($\Delta\Psi_m$)

JC-1 fluorescent probe was used to quickly and sensitively detect the changes of mitochondrial membrane potential in different experimental groups [44]. According to the reagent instructions, the JC-1 fluorescent probe was configured to the working solution concentration, and the working solution of 1 mL was used for the staining of A549 cells in different groups of 10⁵/mL. Incubation at the condition of 37 °C and 5 % CO₂ for 30 min. Afterwards, the JC-1 special buffer was washed to remove the unbound JC-1 fluorescent probe. The fluorescence changes of A549 cells were observed qualitatively and quantitatively by fluorescence microscope and BD FACSCanto II flow cytometry (BD Biosciences).

2.13. Morphological changes of mitochondria by transmission electron microscope (TEM)

The SeNPs@LNT treated A549 cells were washed with PBS. The cells were harvested by centrifugation after trypsinization, then the number of the cells was quantified to 10⁶ by cell counting. The collected cells were fixed with 2.5 % glutaraldehyde for 2 h, and the cells were centrifuged to remove impurities. The glutaraldehyde was added again to fix the cells and place them in 4 °C for later use. Uranium and lead had different electronic staining effects, and the double staining method was generally used for this experiment. After dyeing for 5–10 min, the sections were rinsed with double distilled water, and were checked with TEM.

2.14. ROS generation detection

The detection of cellular oxidative stress was designed by the mechanism that ROS could oxidize non-fluorescent DCFH to fluorescent DCF [45,46]. Fluorescence microscope and fluorescence microplate reader were used to monitor the fluorescence of DCF at 488 nm excitation wavelength and 525 nm emission wavelength, and the level of ROS in A549 cells was detected qualitatively and quantitatively.

2.15. Western blotting analysis

RIPA protein lysate with protease inhibitor and phosphatase inhibitor was used to cleave A549 cells treated with SeNPs@LNT, and non-structural proteins were obtained by centrifugation. Protein concentration was measured by BCA method [47]. The protein of the same quality was transferred to PVDF membrane after electrophoresis. Subsequent to the non-specific protein site blockade, PVDF membrane was combined with specific primary antibody and incubated overnight at 4 °C. TBST eluted the unbound primary antibody, and the PVDF membrane was incubated with HRP-coupled IgG secondary antibody at room temperature for 1 h. The ECL detection kit was used for the color development of WB bands and the expression of target protein was detected on a developing imager.

2.16. In vivo treatment of SeNPs@LNT in mice

There were twenty-four female BALB/c mice at 4–6 weeks old were randomly assigned and formed into four experimental groups: control group, virus group, single SeNPs@LNT treatment group, and virus + SeNPs@LNT treatment group. The mice were anesthetized by intraperitoneal injection for 3 $\mu\text{L/g}$ of 10 % chloral hydrate. The mice in the control group and the single SeNPs@LNT treatment group received 20 μL of normal saline through the nose, and the mice in the Virus group and the virus + SeNPs@LNT treatment group were infected by a titer of 1000 TCID₅₀/mL HAdV-14 through the nose. After 24 h, mice in the single SeNPs@LNT treatment group and the virus + SeNPs@LNT treatment group were fed SeNPs@LNT (0.2 mg Se/kg) through gavage for three consecutive days. The weight and the clinical symptoms of the mice were record every two days. After the mice were euthanized, the blood samples of the mice in each group were collected from the eyeball or heart. The lungs were taken, perfused with normal saline, and fixed with paraformaldehyde for subsequent experiments. The lung tissue of each group of the mice was used for lung index determination, HE staining, TUNEL-DAPI staining, and immunohistochemical staining. The dyeing results were observed by digital microscope (Leica, Germany). After HE staining, the lung tissues of different groups were observed by a digital microscope at 200 \times magnification. The number of cells in each field was counted and analyzed by Image J.

2.17. In vivo treatment of SeNPs@LNT in Se-deficient mice

The Se-deficient mouse model was established through continuous Se-deficient conditions, and the Se-deficient mouse model was tested to ensure that the systemic circulation of the mice was in a state of Se deficiency. Twenty-four female Se-deficient C57BL/6 J mice aged 4–6 weeks were randomly divided into 4 experimental groups: control group, virus group, SeNPs@LNT group, and virus + SeNPs@LNT group. The establishment of the adenovirus pneumonia mouse model was the same as the above method. The body weight and clinical symptoms of the mice were recorded daily. After the mice were euthanized, blood samples from each group of mice were collected from eyeballs or hearts. Lungs were harvested, perfused with saline, and fixed with paraformaldehyde for subsequent experiments. The lung tissues of mice in each group were collected for lung index determination, HE staining, TUNEL-DAPI staining, and immunohistochemical staining. The staining results were observed with a digital microscope (Leica, Germany). The levels of IL-8, IL-12p70, IL-17 A, IL-22, and TNF- β inflammatory cytokines in mouse serum were determined by AimPlex multi-cytokines flow detection technology. The experimental results were acquired from BD FACSCanto II Flow cytometry, and the data was analyzed by FCAP Array v3 software. The relative expression of HAdV-14 DNA in mouse lung tissue lysate was detected by qPCR technology with GADPH as the internal standard. The specific primers used to detect HAdV-14 were as follow: HAdV-14 forward primer, 5'-CAGCAGTCTATGCCCAACAG-3', and HAdV-14 reverse primer, 5'-GCTTGGTCTCCATTTAACTGAATC-3'.

The specific primers used to detect GADPH were as follow: GADPH forward primer, 5'-GCTCCCTCTTTCTTTGCAGC-3', and GADPH reverse primer, 5'- GTTGTATGGATGACCTTGGC-3'.

2.18. Se metabolism of SeNPs@LNT in vivo

Quantitative fresh lung tissue and serum was taken from mice in different treatment groups, and the lung tissue was subjected to nitrification under the heating of mixed acid (VHNO₃:VHClO₄ = 3:1). After the samples were resuspended in 2 % nitric acid solution, Se content in lung tissue was determined by inductively coupled plasma mass spectrometer (ICP-MS, iCAP RQ, Ultimate 3000, Thermo Scientific) [48]. The serum of mice in different treatment groups was separated, and the Mouse GPx1 (Glutathione Peroxidase 1) ELISA Kit (MOES01393, Reagent Genie, Ireland) and the Mouse Thioredoxin Reductase 1/TXNRD-1 ELISA Kit (MOFI01171, Reagent Genie, Ireland) were used for detecting the GPx1 and the Thioredoxin Reductase 1 (TXNRD-1) in the serum by immuno-double antibody sandwich method.

2.19. Statistical analysis

GraphPad Prism v9.0 was used for the display of experimental data, and IBM SPSS Statistics v26.0 was used for statistical analysis of experimental data. The data of each experimental group were counted by mean \pm SEM. Double-tailed student t-test and one-way ANOVA were used for comparison between the two groups and multiple groups. The statistical differences were further classified according to the *P* value, such as *P* < 0.05 (*), *P* < 0.01 (**), *P* < 0.001 (***) or *P* < 0.0001 (****).

3. Results and discussion

3.1. Design, preparation, and characterization of SeNPs@LNT

Scheme 1 systematically demonstrated the rationality of designing SNPs@LNT in animal and cellular models for the treatment of adenovirus pneumonia caused by HAdV-14 infection. We found that the size distribution of SeNPs@LNT was normally distributed with PDI was 0.171 (**Fig. 1A**). Simultaneously, the average size and zeta potential of SeNPs@LNT was 125.5 \pm 2.65 nm and -13.9 ± 0.62 mV, respectively (**Fig. 1A**), while the zeta potential of SeNPs was -7.95 mV (**Fig. S1**). Further, the TEM image shown the diameter of SeNPs@LNT was about 90 nm (**Fig. 1B**). The slight aggregation of SeNPs@LNT and its surrounded liquid layer within water are the main contributors for the significant discrepancy. More importantly, we further used XPS to analyze the structure of SeNPs@LNT (**Fig. 1C**). O 1s at 532.88 eV and 536.73 eV was present in the spectrum of LNT, while Se 3d at 56.38 eV, 58.38 eV and 60.43 eV were present in SeNPs. Both O 1s at 531.73 eV/533.18 eV/538.28 eV and Se 3d at 55.83 eV were observed in SeNPs@LNT, demonstrated that Se–O bond was presented in SeNPs@LNT particles, which accounting for the stability of SeNPs@LNT particles (**Fig. 1D–E**). These results demonstrated that the SeNPs@LNT was synthesized successfully.

3.2. In vitro antiviral activity of SeNPs@LNT

The cytotoxicity of SeNPs@LNT was assessed by CCK-8 assay. When the concentration of SeNPs@LNT reached 16 μM , the cell viability decreased significantly to below 90 %. However, SeNPs@LNT showed low cytotoxicity to A549 cells in the concentration range of 1–8 μM , and the cell viability of A549 cells was all higher than 90 % (**Fig. 1F–G**). So that SNPs@LNT in this concentration range was selected to test the antiviral efficiency. In order to directly study the inhibitory effect of SeNPs@LNT on HAdV-14 infection in A549 cells, the HAdV-14 virus strain RAD14EGFP with eGFP gene was used in this experiment. After the A549 cells infected by rAD14 EGFP were treated with different concentrations of SeNPs@LNT, the fluorescence morphology of A549

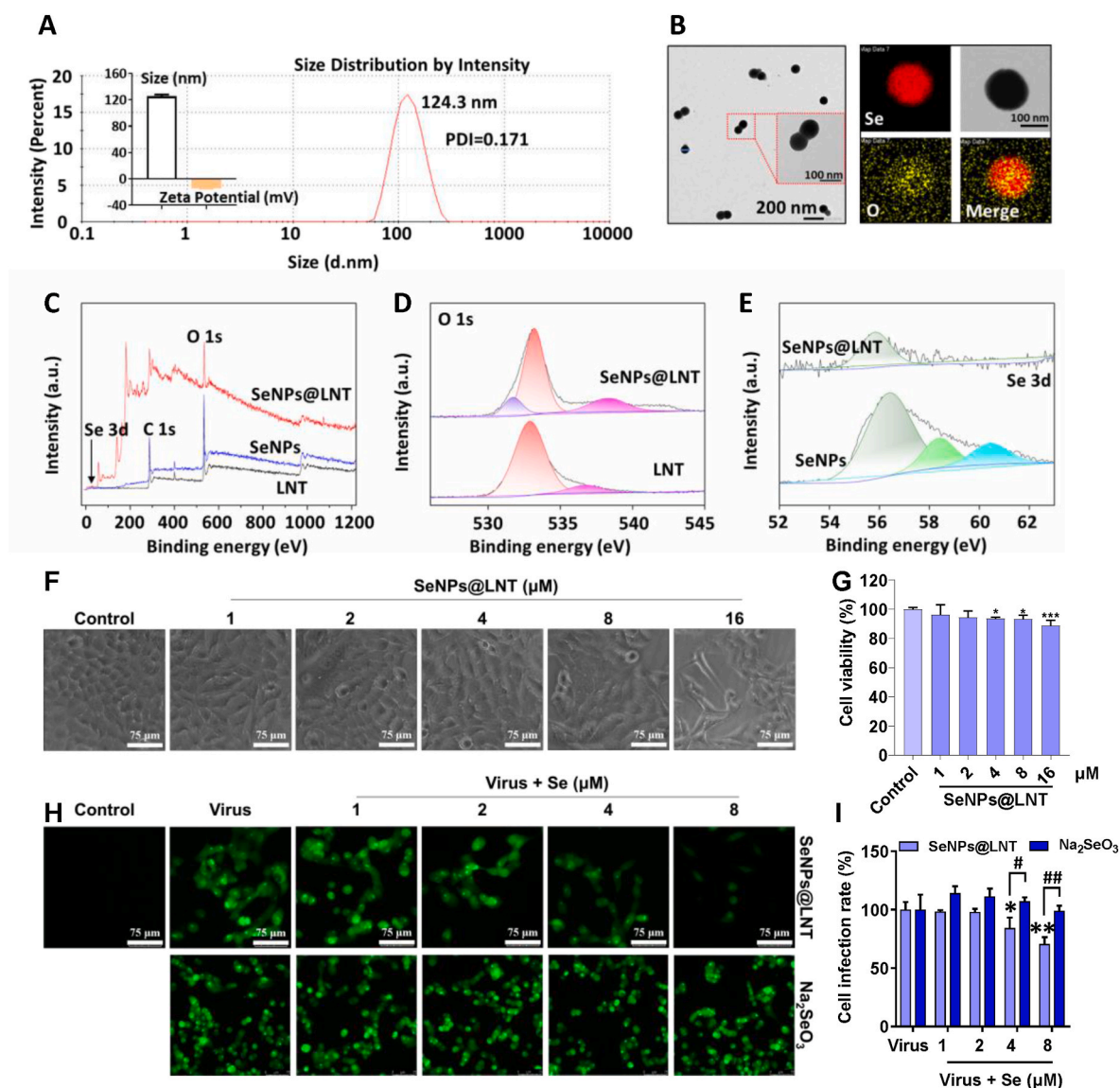


Fig. 1. Design, preparation and characterization of the SeNPs@LNT, and the optimal antiviral concentration of SeNPs@LNT. (A) Hydrodynamic size distribution diagram and zeta potential of SeNPs@LNT; (B) TEM image of SeNPs@LNT; (C) The XPS spectrum of LNT, SeNPs and SeNPs@LNT; (D) The binding energy of O 1s in LNT and SeNPs@LNT; (E) of Se 3d in SeNPs and SeNPs@LNT; (F) Cytotoxicity and (G) quantitative analysis of SeNPs@LNT at a range of concentrations from 1 to 16 μM on A549 cells. The cell viability of A549 cells treated with different concentrations of SeNPs@LNT was detected by CCK-8 assay; (H) Fluorescent morphological changes, fluorescence intensity changes (I) and quantitative analysis in rAD14 EGFP-infected A549 cells after treatment with SeNPs@LNT or Na_2SeO_3 . Error bars represent the confidence interval for the mean ($n = 3$) at the 95 % level. SeNPs@LNT treated A549 cells for 48 h. Bars with different characters are statistically different at $P < 0.05$ (* or #), $P < 0.01$ (** or ##), or $P < 0.001$ (***) level. * represents comparison with the Control group, # represented comparison with the Control or Virus group.

cells could be measured under fluorescence microscope. As shown in Fig. 1H–I, A549 cells infected with rAD14 EGFP showed obvious CPE, and the infected cells emitted green fluorescence with strong fluorescence intensity, indicating that lots of cells were infected by the virus. When rAD14 EGFP replicated and assembled into virus particles, the inserted eGFP gene expressed green fluorescent protein along with the replication of the virus. The increased fluorescence intensity in the infected cells indicated a high intracellular viral load. After SeNPs@LNT treatment, the number of fluorescent cells decreased and the fluorescence intensity decreased with the increase of drug concentration. In addition, the fluorescence intensity can also be achieved by multi-point fluorescence detection. When A549 cells infected by HAdV-14 were treated with 1–4 μM SeNPs@LNT, the fluorescence intensity was 98.4 %, 97.9 % and 84.2 %, respectively, while the fluorescence intensity of group 8 μM SeNPs@LNT decreased significantly to 70.6 %, indicating

that SeNPs@LNT improved antiviral efficiency in a dose-dependent manner. Furthermore, 8 μM was the optimal antiviral concentration with low toxicity, and the following experiments were performed with 8 μM SeNPs@LNT. We also conducted experiments on sodium selenite (Na_2SeO_3) against HAdV14. It was found that there was no significant difference in fluorescence intensity, compared HAdV14 + Na_2SeO_3 group to the HAdV14 control group, indicating that Na_2SeO_3 did not have an anti- HAdV14 effect (Fig. 1H–I). Collectively, these results indicated that SeNPs@LNT significantly inhibited the infection rate of HAdV-14 in A549 cells.

3.3. Assessment of antiviral activity from detecting the virulence of progeny virus after SeNPs@LNT treatment

Benefit from the rAD14 EGFP that expressed eGFP, the infection rate

of HAdV-14 in A549 cells could be observed by phase-contrast microscopy and fluorescence microscopy. As known as Fig. 2A–B, the titer of the primary virus group was $4.3 \text{ Log}_{10} \text{ TCID}_{50}$, while the viral titer of the progeny virus group was $1.5 \text{ Log}_{10} \text{ TCID}_{50}$. Most surprisingly, the virulence test of the supernatant in the virus + SeNPs@LNT group found that progeny virus treated with SeNPs@LNT in the supernatant of each dilution gradient caused no virus infection to A549 cells. As well as this result was consistent with the observations by phase-contrast microscopy and fluorescence microscopy. These data inferred that SeNPs@LNT effectively reduced the production of progeny virus by HAdV-14, thereby significantly reducing the cell damage caused by the progeny virus. The mechanism might be that SeNPs@LNT inhibited the replication of viral DNA to reduce the synthesis of progeny virus particles, and finally reduced the burden of the virus on the host cell material metabolism.

3.4. Intracellular and extracellular detection of viral load of HAdV-14

Intracellular and extracellular HAdV-14-specific DNA was detected by qPCR in different treatment groups, and RPL-18 was used as an internal standard for relative quantification. As shown in Fig. 2C–D, there was no significant difference in the relative expression levels of HAdV-14-specific DNA in the culture supernatant between the virus group and the virus + SeNPs@LNT group. However, the relative expression of HAdV-14-specific DNA in A549 cells in the virus + SeNPs@LNT group

was significantly lower than that in the virus group, which demonstrated that SeNPs@LNT effectively reduced the viral load of HAdV-14 in A549 cells. It was speculated that the antiviral effect of SeNPs@LNT was to inhibit the transport, replication, and proliferation of the virus in cells, and to repair the intracellular metabolic disorder caused by the virus.

3.5. Translocation of HAdV-14 in A549 cells

In the early stage of viral invasion (0–6 h), there was no obvious CPE in the cells, and green fluorescence was scattered in the cytoplasm and overlapped with the red fluorescence of labeled lysosomes (Fig. 3A). This result suggested that the virus was transported in the cytoplasm after infecting cells, and might undergo structural changes under the action of lysosomes, such as detaching from endosomes and releasing viral particles for subsequent infection. This was consistent with previous studies [49]. The CPE of the cells and the intensity of green fluorescence gradually increase over time. With the development of viral infection (12 h–30 h), the green fluorescence expressed by the virus tended to accumulate in the nucleus area, and the green fluorescence intensity in the nucleus area increased significantly (Fig. 3A). The result suggested that HAdV-14 might aggregate in the host nucleus, and then released viral DNA and replicated. Since HAdV-14 could synthesize viral DNA by inhibiting or utilizing the nucleic acid synthesis mechanism of host cells, it might cause metabolic disorders of cellular nucleic acids and proteins to a certain extent. Furthermore, HAdV-14 might mediate

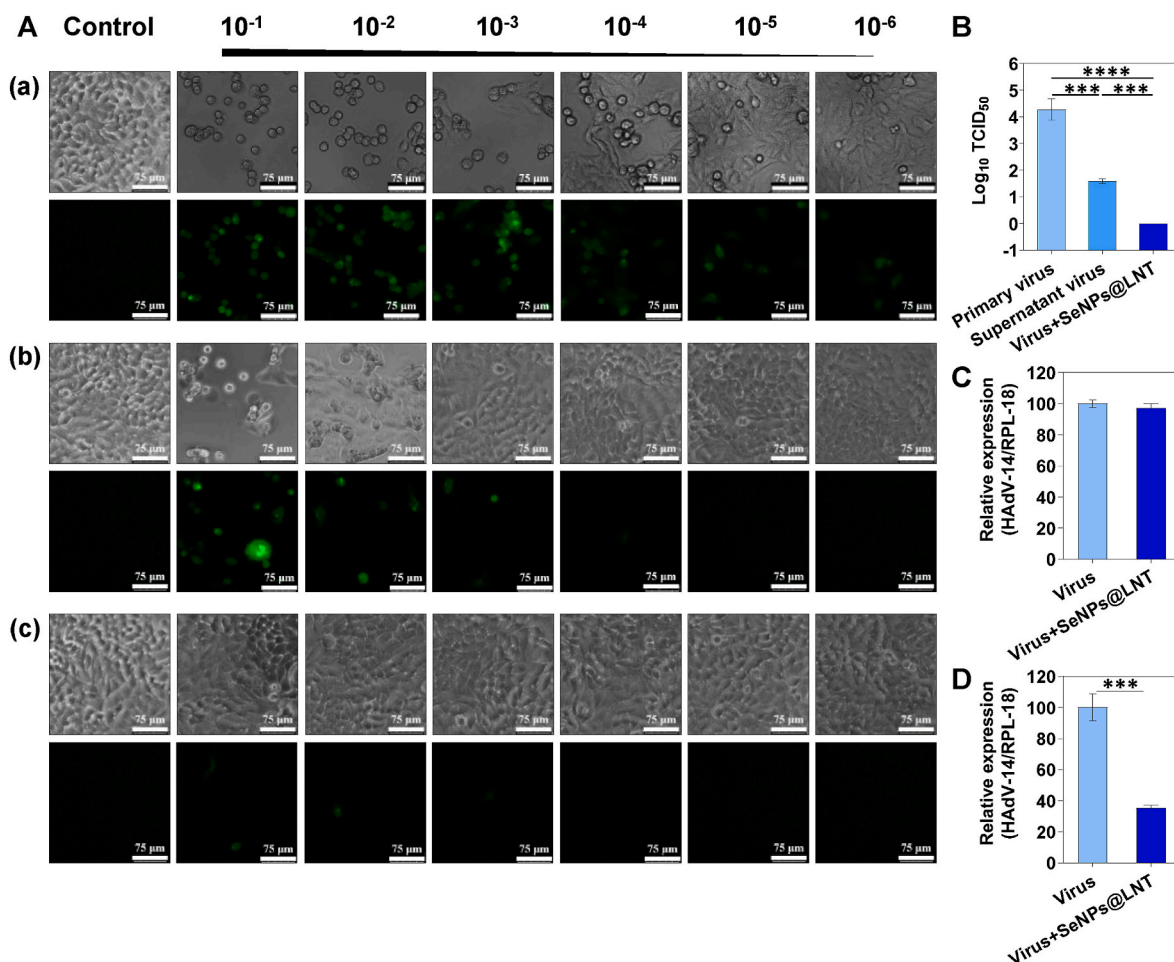


Fig. 2. Evaluation of HAdV-14 viral load and progeny virus virulence after SeNPs@LNT treatment. (A and B) Assessment of the virulence of progeny virus after SeNPs@LNT treatment by TCID_{50} assay. (a) A549 cells infected by primary virus; (b) A549 cells infected by progeny virus; (c) A549 cells infected by progeny virus were treated with SeNPs@LNT; (C) There was no significant difference in the relative expression of the HAdV-14-specific DNA in the culture supernatant between the virus group and the virus + SeNPs@LNT group; (D) The relative expression of the HAdV-14-specific DNA in A549 cells of the virus + SeNPs@LNT group was significantly reduced compared with the virus group. Bars with different characters are statistically different at $P < 0.001$ (***) or $P < 0.00001$ (****) level.

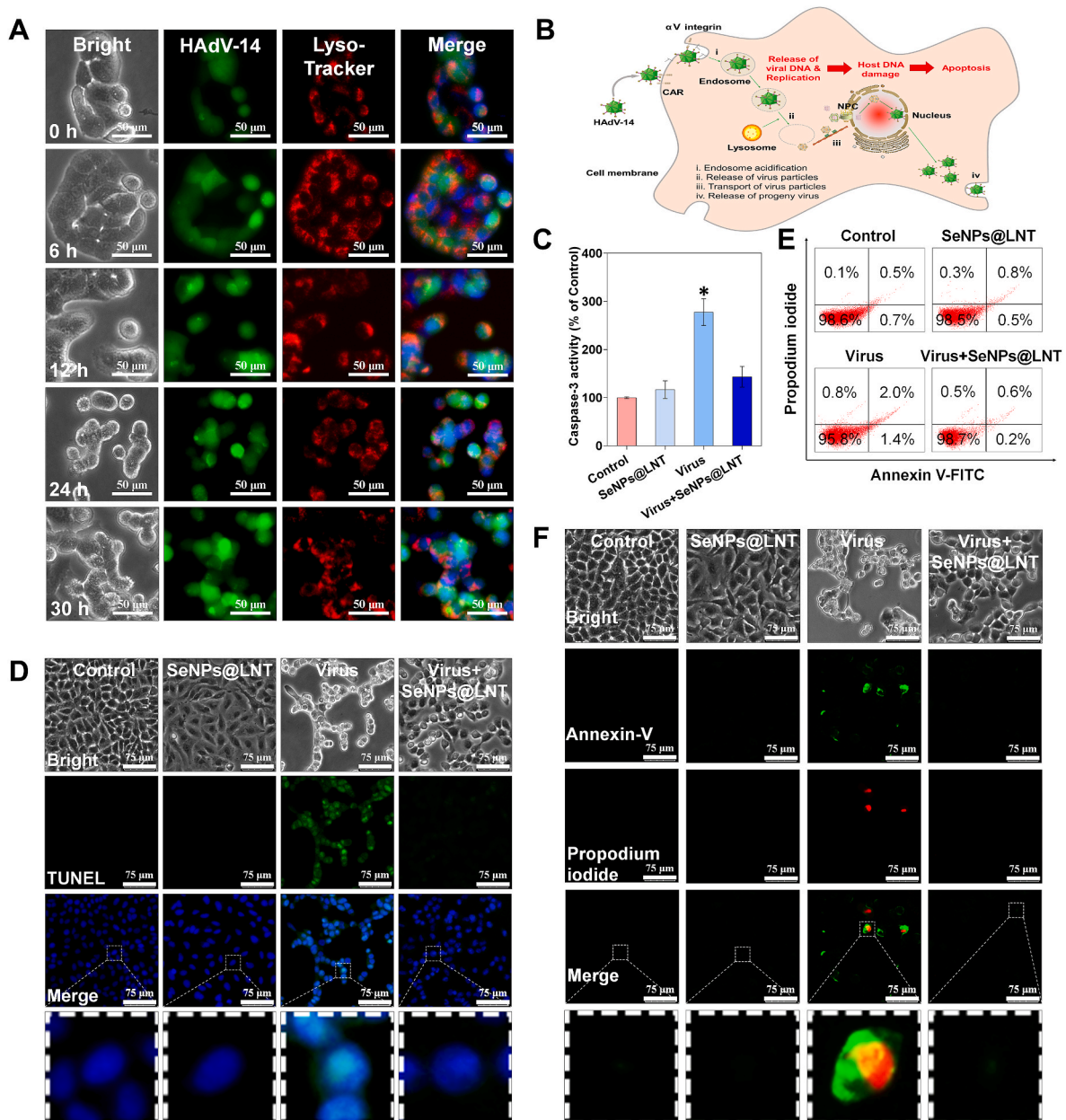


Fig. 3. Intracellular localization of HAdV-14 and the inhibitory effect of SeNPs@LNT on apoptosis induced by HAdV-14 infection. (A) DAPI was used for nuclear staining and Lyso-tracker was used for lysosome staining. The A549 cells were infected by rAD14 EGFP for different periods and were observed under the fluorescent microscope; (B) Schematic diagram of the infection process of HAdV-14 in A549 cells; (C) HAdV-14 infection of A549 cells were treated with SeNPs@LNT and the caspase-3 activity was detected by the absorbance of pNA; (D) DNA fragmentation and nuclear deformation in A549 cells were detected by TUNEL-DAPI co-staining assay; (E and F) A549 cells in each group were stained with Annexin V-FITC and PI to detect phosphatidylserine on the cell membrane surface. The results of fluorescent labeling were observed by flow cytometry and fluorescence microscopy. The A549 cells were treated with 8 μ M SeNPs@LNT for 48 h. Bars with different characters are statistically different at $P < 0.05$ (* or #) level. * represents comparison with the Control group, # represented comparison with the Virus group.

the genomic DNA damage by invading the nucleus (Fig. 3B).

3.6. Inhibition of caspase-3 activation and DNA fragmentation by SeNPs@LNT improves apoptosis

Caspase-3 was a protease that play an irreplaceable role in the process of cell apoptosis. The abnormal expression of caspase-3 might lead to the disorder of procedural cell apoptosis. As shown in Fig. 3C, the caspase-3 activity of A549 cells infected by HAdV-14 was obviously increased to 277.79 %, while the caspase-3 activity of SeNPs@LNT treatment group was significantly decreased to 143.41 %. Caspase-3 was a potent apoptosis-inducing enzyme that catalyzed the specific cleavage

of many pivotal cellular proteins. Caspase-3 cleaved key cellular proteins in apoptosis through a cascade effect that transmitted apoptosis signals from cell-surface-based death receptors to a series of caspases. During the induction of apoptosis, caspase-3 played an integral role in chromatin condensation and DNA fragmentation. Our results demonstrated that SeNPs@LNT effectively inhibited the activity of caspase-3, indicating that SeNPs@LNT might regulate the abnormal apoptosis caused by HAdV-14 through the caspase-3-mediated signaling pathway.

Benefit from the experimental results above, after HAdV-14 infected A549 cells, it aggregated in the nucleus, and conducted DNA replication and protein synthesis. HAdV-14 could up-regulate the activity of caspase-3 to a certain extent, and might cause DNA damage in

chromosomes in the process of inducing apoptosis. To examine the status of DNA in the nucleus, TUNEL-DAPI co-staining assay was performed on A549 cells in different groups. A549 cells infected with HAdV-14 showed obvious CPE, the nucleus was deformed and the DNA in the nucleus was fragmented (Fig. 3D). The experimental results showed that SeNPs@LNT effectively restored the morphology of the nucleus to a certain extent and inhibited the DNA fragmentation caused by HAdV-14 infection.

The early apoptotic cells were positive for Annexin V-FITC staining and negative for PI staining. There were 0.7 % and 0.5 % of early apoptotic cells in the control group and the SeNPs@LNT group, respectively (Fig. 3E). However, the early apoptotic cells in the virus group accounted for 1.4 %, and the early apoptotic cells in the virus + SeNPs@LNT group decreased to 0.2 % (Fig. 3E). The late stage of apoptotic cells was double positive for Annexin V-FITC staining and PI staining. The control group and the SeNPs@LNT group had 0.5 % and 0.8 % late apoptotic cells, respectively, while the virus group had a late apoptotic rate of 2.0 % (Fig. 3E). However, the late apoptotic rate of the virus + SeNPs@LNT group was significantly reduced to 0.6 % (Fig. 3E). The changes in intracellular fluorescence were observed by the fluorescence microscope and flow cytometry, and the CPE of A549 cells were observed by the optical microscope. Cells with obvious CPE in the virus group showed the phenomenon of phosphatidylserine eversion, and some cells had enhanced permeability. After SeNPs@LNT treatment, the phenomenon of early and late apoptosis was significantly reduced (Fig. 3F). In conclusion, our data showed that SeNPs@LNT could effectively inhibit the cellular early and late apoptosis caused by HAdV-14 infection.

3.7. SeNPs@LNT repairs ROS-mediated mitochondrial dysfunction induced by HAdV-14 infection

The change of JC-1 probe from red fluorescence to green fluorescence was used to evaluate the decrease of mitochondrial membrane potential ($\Delta\Psi_m$) in A549 cells, which reflected the functional state of mitochondria and suggested the early apoptosis signal. As shown in Fig. 4A, the transition from red fluorescence in PE fluorescence channel to green fluorescence in FITC fluorescence channel was monitored by flow cytometry. There were 25.6 % of red fluorescence turned to green fluorescence in control group, and 56.1 % of red fluorescence turned to green fluorescence in virus group. After treatment with SeNPs@LNT, only 37 % of the red fluorescence in the virus + SeNPs@LNT group turned to green fluorescence. As shown in Fig. 4B, the JC-1 probe in the control group entered the mitochondria and showed high intensity red fluorescence signals mainly in the presence of aggregate. However, mitochondrial depolarization occurred in A549 cells infected with HAdV-14, and the JC-1 probe was transformed into monomer form in cytoplasm, which changed from red fluorescence to high intensity green fluorescence. SeNPs@LNT treatment significantly reversed the mitochondrial depolarization induced by HAdV-14 infection in A549 cells, showing a decrease in green fluorescence intensity and an increase in red fluorescence intensity. These results demonstrated that HAdV-14 infection might mediate mitochondrial dysfunction. Mitochondria were involved in the oxidative phosphorylation reaction, which was the site of oxidative metabolism in cells and had the ability to regulate the cell cycle. HAdV-14 infection might cause the performance of mitochondria to decline through oxidative stress, and lead host cells abnormally enter the apoptosis stage. Therefore, SeNPs@LNT resisted HAdV-14 infection mainly by maintaining the stability of mitochondrial state

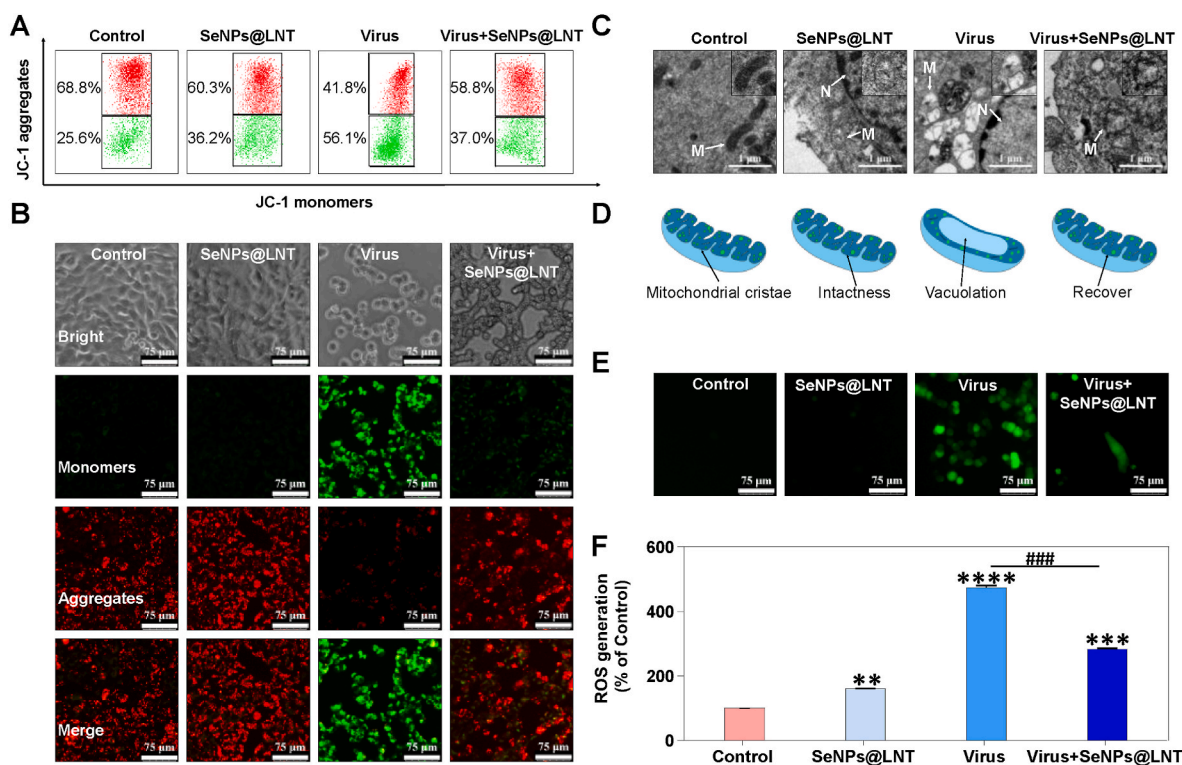


Fig. 4. SeNPs@LNT repairs mitochondrial dysfunction and reduces ROS overproduction induced by HAdV-14 infection. (A, B) SeNPs@LNT inhibited apoptosis in HAdV-14 infection of A549 cells. Mitochondrial membrane potential changes were detected by mitochondrial membrane potential assay kit with JC-1; (C, D) SeNPs@LNT repaired the damage and deformation of mitochondria induced by HAdV-14 infection in A549 cells. N: nucleus; M: mitochondria; (E) The levels of ROS in A549 cells of different groups could be detected by monitoring the fluorescence of DCF and the green fluorescence produced by ROS was detected by a fluorescence microscope; (F) The quantitative fluorescence intensity of ROS was detected by a fluorescence microplate reader. The A549 cells were treated with 8 μM SeNPs@LNT for 48 h. Bars with different characters are statistically different at $P < 0.01$ (**), $P < 0.001$ (*** or ###), or $P < 0.00001$ (****) level. * represents comparison with the Control group, # represented comparison with the Virus group.

and regulating apoptosis.

After a series of operations such as fixation, dehydration, embedding, and sectioning of A549 cells, the morphology of mitochondria in the different groups was observed by TEM. As shown in Fig. 4C–D, the mitochondria in the cells of the control group were oval with obvious cristae structure. In the virus group, the mitochondria within the cells found obvious deformation, such as swelling, light staining, and the cristae structure became shorter and shifted. In addition, the presence of blank areas in the mitochondria indicated that the mitochondrial matrix was dissolved. However, in the SeNPs@LNT treatment group, the mitochondria recovered the obvious double-layer membrane structure and the cristae structure appeared. The results show that SeNPs@LNT could effectively repair the damage of mitochondria. Mitochondrion, an organelle that was extremely sensitive to damage, and changes in mitochondrial morphology could reflect the functional changes caused by mitochondrial damage to a certain extent. ROS was one of the by-products of molecular oxygen produced by mitochondrial oxidative phosphorylation. Oxidative stress occurred when there was an imbalance between ROS metabolism and antioxidant defense system. We speculated that the antiviral effect of SeNPs@LNT was related to the repair of mitochondria that undergo oxidative stress.

Intracellular ROS could oxidize non-fluorescent DCFH into fluorescent DCF. The detection of DCF fluorescence effectively reflected the production of ROS, which was used to explain the state of intracellular oxidative stress. As shown in Fig. 4E, there was no significant difference in fluorescence intensity between the control group and the SeNPs@LNT group, but viral infection significantly increased the production of intracellular ROS. The fluorescence intensity of virus + SeNPs@LNT group remarkably decreased compared with the virus group. What's more, the fluorescence intensity of the SeNPs@LNT group was slightly different from the control group. The specific fluorescence intensity of DCF in different groups was detected semi-quantitatively by fluorescence microplate instrument. Compared with the control group, the fluorescence intensity of the virus group significantly increased to 474.3 %, while that of the virus + SeNPs@LNT group decreased to 283.8 %, as shown in Fig. 4F. ROS was important molecule in physiological processes and contributed greatly to the homeostasis of redox reactions in the body, especially apoptosis signaling, cell proliferation, and immune

system maintenance. Once ROS was overproduced, it would lead to an imbalance of basic redox metabolism, resulting in excessive oxidative stress. Oxidative stress gave rise to ROS-mediated direct or indirect damage to nucleic acids, proteins, and lipids, and this damage mechanism was associated with a variety of pathological conditions [50]. The results suggested that the decrease in ROS might be involved in the antiviral effect. HAdV-14 infection led to excessive ROS production, activating a potent oxidative stress response. From the experimental results, it is speculated that oxidative stress might cause DNA damage and activate a series of apoptosis signaling pathways. After SeNPs@LNT treatment, ROS-mediated cell damage and apoptotic activity were reduced to counteract the damage caused by the virus.

3.8. Regulation of ROS-mediated apoptosis signaling pathway by SeNPs@LNT

As obtained from previous experiments, mitochondria, as the main site of cellular oxidative metabolism, could regulate the cell cycle to a certain extent. HAdV-14 infection led to mitochondrial dysfunction, and the oxidative stress response in the host cells was unbalanced. Ultimately, the host cells entered the apoptotic stage. SeNPs@LNT inhibited the mitochondria-induced apoptosis (Fig. 5A). In the process of mitochondrial oxidative stress, the regulatory functional proteins Erk1/2, Akt, Bcl-xL and Bcl-2 played an important role in inhibiting excess ROS-mediated apoptosis signaling pathway. Especially Bcl-xL and Bcl-2 stayed in the outer membrane of the mitochondria, and inhibited the release of cytochrome C, in order to prevent cytochrome C combine with APAF-1. Furthermore, cytochrome C could form an activation complex with caspase family, resulting in a cascade reaction to activate apoptotic proteins such as PARP to induce apoptosis [51,52]. Bad was a member of the pro-apoptotic family of Bcl-2 signaling pathways, which promoted apoptosis by blocking the binding function of Bcl-2 and Bcl-xL. Akt and Erk1/2 prevented the binding of Bad to Bcl-2 and Bcl-xL by phosphorylating Bad, and inhibited the apoptotic activity of Bad [53]. As shown in Fig. 5B, HAdV-14 infection led to a decreased expression of Bcl-xL and Bcl-2 proteins and increased expression of Bad protein. After treatment with SeNPs@LNT, the expression of Bad protein was down-regulated while the expression of Bcl-xL and Bcl-2 proteins was up-regulated. In

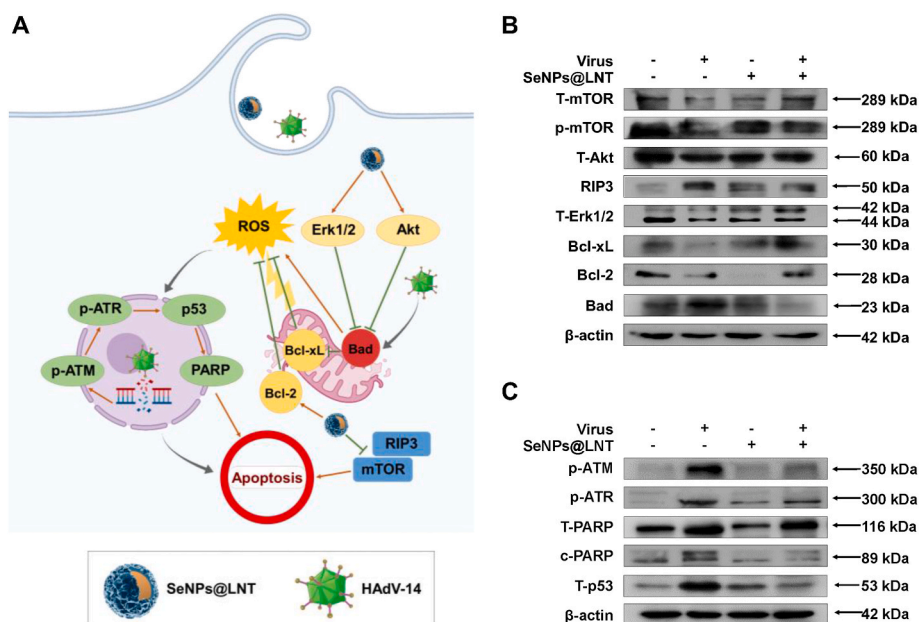


Fig. 5. Regulation of SeNPs@LNT on oxidative stress response and DNA damage-mediated apoptosis signaling pathway caused by HAdV-14 infection. (A) The sketch of apoptotic signaling pathways participated in the antiviral activities of HAdV-14 by SeNPs@LNT; (B) Regulation of apoptotic proteins in the Bcl-2 signaling pathways by SeNPs@LNT; (C) Regulation of DNA damage proteins in the p53 signaling pathways by SeNPs@LNT. The A549 cells were treated with 8 μ M SeNPs@LNT for 48 h.

addition, the expression levels of p53, PARP, c-PARP (Asp214), p-ATM (Ser1981) and p-ATR (Ser428) in the virus + SeNPs@LNT group were significantly lower than those in the virus group (Fig. 5C). Benefit from the above experimental results, we found that in the process of HAdV-14 infection, HAdV-14 would aggregate in the nucleus to complete viral DNA replication and proliferation. In order to explore whether HAdV-14 would damage the host cell, especially the DNA in the nucleus, when HAdV-14 conducted the viral particle synthesis, we examined the DNA state in the nucleus. The experiments found that HAdV-14 infection could cause damage to cellular DNA. The PARP-related signaling pathway caused apoptosis mediated by DNA damage, which was consistent with our experimental conclusions [54]. DNA damage could lead to the phosphorylation of ATM and ATR, and the activated p-ATR (Ser428) protein upregulated the expression of p53 protein, and finally form a p53 and PARP-mediated apoptosis pathway. The p53 and PARP proteins also participated in the ROS-related caspase-3 cascade reaction to further promote apoptosis [55,56]. Compared with the virus group, the virus + SeNPs@LNT group remarkably increased the expression levels of mTOR and p-mTOR (Ser2448), and reduced the expression level of RIP3, as shown in Fig. 5B. The mTOR and RIP3 signaling pathways could promote material metabolism, participate in cell apoptosis, autophagy, and play a non-negligible role in life cycle. The results indicated that the signaling pathway composed of functional proteins including Erk1/2, Akt, Bad, Bcl-xL, Bcl-2, p53, PARP, ATM, ATR, mTOR and RIP3 was involved in the restriction of apoptosis by SeNPs@LNT. In the *in vitro* cellular model, HAdV-14 infection resulted

in excessive mitochondrial production of ROS and caused cellular DNA damage. SeNPs@LNT effectively inhibited HAdV-14-induced host cell apoptosis in a specific signaling pathway, as shown in Fig. 5A.

3.9. Alleviation of inflammation and DNA damage-mediated apoptosis in mice treated with SeNPs@LNT

Since SeNPs@LNT effectively suppressed HAdV-14 infection in the A549 cell model, we next evaluated the therapeutic effect of SeNPs@LNT in mice. As shown in Fig. 6A–C, after the mice in the virus group were infected with HAdV-14 through nose drops, there was no significant change in the body weight of the mice, but the lung index was significantly higher than that in the control group. Inflammation in the lungs might cause the proportion of lung weight increased, suggesting that the animal model of pneumonia caused by HAdV-14 infection was successfully replicated. Compared with the virus group, the virus + SeNPs@LNT group could significantly reduce the lung index of mice with pneumonia (Fig. 6B). Furthermore, there was no significant difference in body weight of the mice between the SeNPs@LNT group and control group, which proved that SeNPs@LNT had excellent safety and effectiveness in animal models. The increase in the lung index of the mice indicated that the lungs of the mice developed inflammation after HAdV-14 infection, and the reactive proliferation of inflammatory cells and tissue cells caused the lungs swelling.

In order to visually observe the morphological changes and inflammatory responses of the lung tissue from mice in different groups, lung

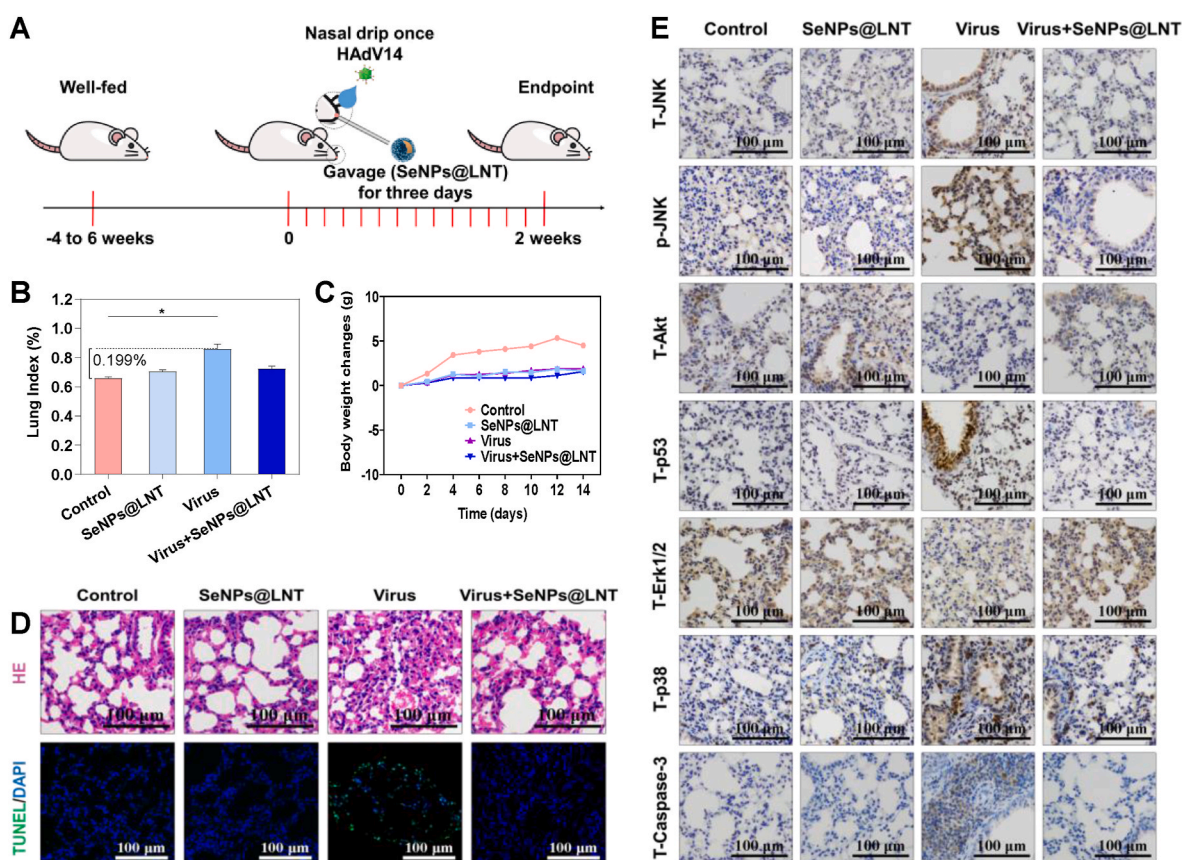


Fig. 6. SeNPs@LNT resists adenovirus pneumonia induced by HAdV-14 in mice. (A) Schematic showing the *in vivo* experimental design for the treatment of HAdV-14 infection; (B) Analysis of lung index in mice treated with SeNPs@LNT. After the mice in the virus group were infected with HAdV-14 through nose drops, the lung index was significantly higher than that in the control group; (C) Survival and body weight of mice in different groups at 14 d; (D) The lung tissue sections of mice in different treatment groups were stained with HE and the number of cells in each field was counted and analyzed by Image J. TUNEL test was performed on the lung tissue of mice to detect the DNA fragmentation; (E) Immunohistochemistry of the mice in different groups. The dark brown particles representing T-p38, T-p53, T-JNK, p-JNK (Thr183/Tyr185), T-Caspase-3, T-Akt, and T-Erk proteins expression in the lung tissue of the mice. The therapeutic concentration of SeNPs@LNT was 0.2 mg Se/kg. Bars with different characters are statistically different at $P < 0.05$ (* or #) or $P < 0.01$ (**) level. * represents comparison with the Control group, # represented comparison with the Virus group.

tissue sections of the mice in different groups were used for HE staining. As shown in Fig. 6D, compared with the control group, the mice in the virus group exuded a large number of inflammatory cells in the lung parenchyma, and the lung tissue structure collapsed. There were a mass of tissues and epithelial cell proliferation in the lung, and the alveolar size was heterogeneous. In the virus + SeNPs@LNT group, lung inflammation was improved, manifested by reduced lung tissue exudation, and decreased inflammatory cell numbers as shown in Fig. 6D. Meanwhile, the alveolar structure returned to normal vacuolar shape. We speculated that in the mouse lungs, SeNPs@LNT inhibited HAdV-14 infection by reducing the replication and proliferation of HAdV-14. Since the pathogenic source of adenovirus pneumonia was suppressed, the symptoms of inflammatory cell aggregation and tissue compensatory inflammatory hyperplasia caused by pneumonia were alleviated. In

order to verify whether the mechanism of adenovirus-induced damage to mouse lung tissue was consistent with *in vitro* cell models, the lung tissue from mice in different groups was used for TUNEL-DAPI test to detect DNA fragmentation in the nucleus. Similar to the experimental results on the cell models, HAdV-14 infection could cause DNA damage in the nucleus of the mouse lung tissue. However, SeNPs@LNT effectively repaired the DNA damage in the lungs of mice caused by HAdV-14 infection (Fig. 6D). The results directly demonstrated the function of SeNPs@LNT to regulate apoptosis in lung tissue by inhibiting viral infection-mediated DNA damage.

The results of *in vitro* cell models showed that the damage caused by HAdV-14 infection was closely related to apoptosis. In order to deeply explore the molecular biological mechanism of SeNPs@LNT against HAdV-14 infection, immunohistochemical staining were performed of

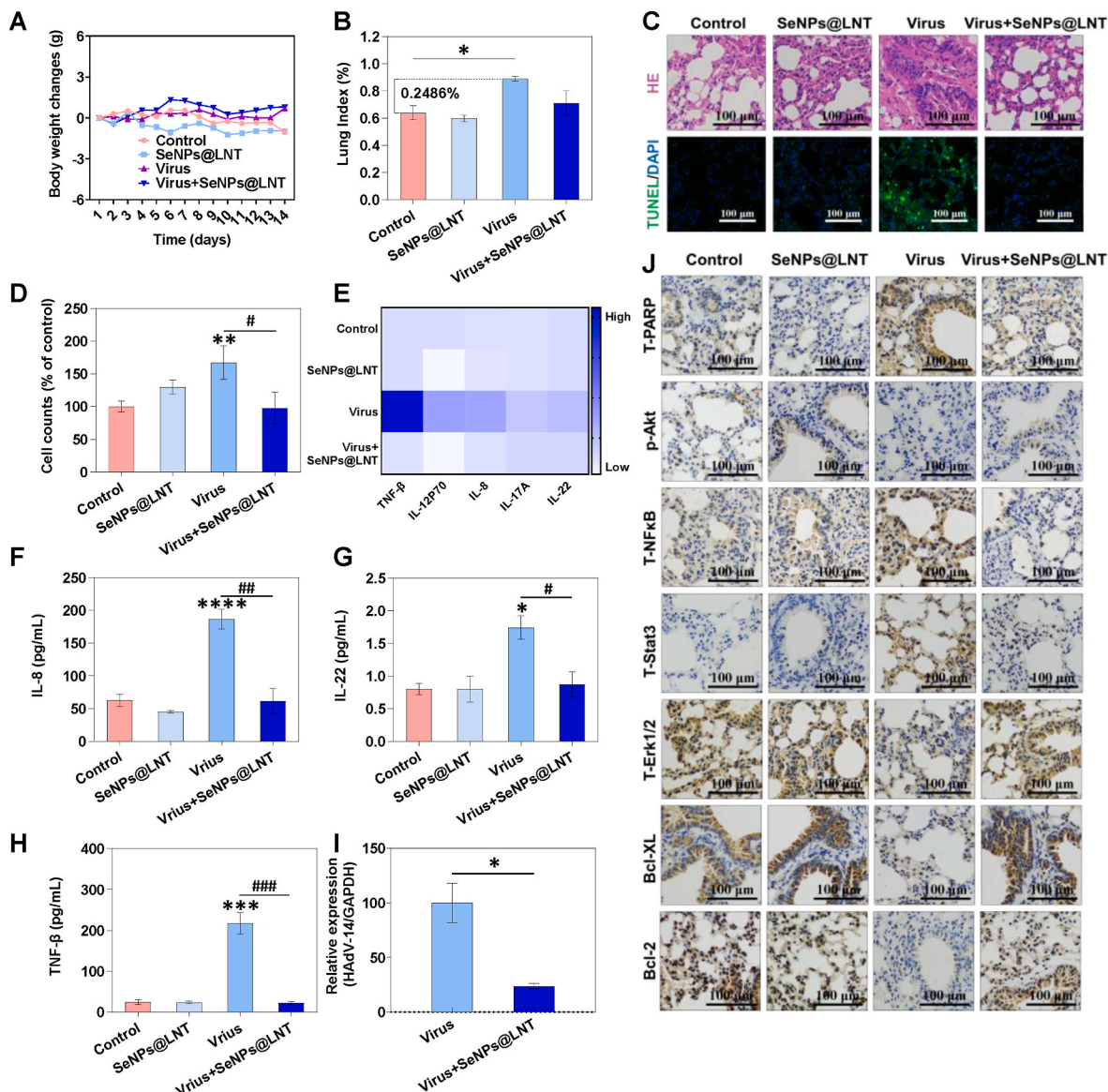


Fig. 7. SeNPs@LNT inhibits inflammatory cytokine storm-mediated apoptosis in Se-deficient mice. (A) Survival rate and body weight of mice in different groups at 14 days; (B) Analysis of lung index of mice in different groups; (C, D) HE staining of lung tissue sections of mice in different groups to observe lung tissue morphology and inflammatory cell proliferation. TUNEL/DAPI staining of lung tissue sections of mice in different groups to detect DNA fragmentation damage in lung tissue and cells; (E–H) The heat map showed the changes in the expression of IL-8, IL-12p70, IL-17 A, IL-22, and TNF-β inflammatory cytokines in the serum of mice in each group; (I) qPCR technology was used to detect the relative expression of HAdV-14-specific DNA in lung tissue of mice in different groups; (J) Immunohistochemical staining of mice in different groups. Dark brown particles represent the expression of T-PARP, p-Akt (Ser473), T-NFκB, T-Stat3, T-Erk1/2, Bcl-xL, and Bcl-2 proteins in mouse lung tissue. The therapeutic concentration of SeNPs@LNT was 0.2 mg Se/kg. Bars with different characters are statistically different at $P < 0.05$ (* or #), $P < 0.01$ (##), $P < 0.001$ (***), or $P < 0.0001$ (****) level. * represents comparison with the Control group, # represented comparison with the Virus group.

lung tissue from mice in different groups. By detecting the expression of proteins on the signaling pathways that promoted and inhibited apoptosis, the results showed that compared with the control group, the expression of pro-apoptotic proteins in the virus group was significantly increased including T-p38, T-p53, T-JNK, p-JNK (Thr183/Tyr185), T-Caspase-3. Meanwhile, the expression of apoptosis inhibitory proteins was significantly down-regulated, such as T-Akt and T-Erk1/2. However, the expression of pro-apoptotic proteins in the virus + SeNPs@LNT group was significantly lower than that in the virus group, while the expression of apoptosis-inhibiting proteins was higher than that in the virus group (Fig. 6E). The apoptosis regulatory proteins T-p53, T-Akt, T-Erk1/2 and T-Caspase-3, which were detected in A549 cell model, were consistent with the regulation of apoptosis signal pathway in mouse lung tissue. We speculated that the difference in experimental results might be that A549 cells were a single type of lung cells, whereas lung tissue was composed of different types of alveolar cells, epithelial cells, connective tissue, and abundant capillaries. Therefore, the changes of apoptosis-regulating proteins in the *in vivo* animal models might be under the influence of adenovirus pneumonia on the homeostasis of the internal environment, reflecting the protein expression rules of multi-cell and tissue.

3.10. SeNPs@LNT treatment inhibits inflammatory cytokine storm-mediated apoptosis in Se-deficient mice

In order to further explore the mechanism of Se in the adenovirus pneumonia mouse model, we established a Se-deficient mouse model to study the therapeutic mechanism of SeNPs@LNT. After the Se-deficient mice in the virus group were infected with HAdV-14 by intranasal instillation, the body weight of the mice did not change significantly, but the lung index was significantly higher than that of the control group, and the lung index decreased after SeNPs@LNT treatment (Fig. 7A and B). Meanwhile, compared with the normal mice (0.199 %), the lung index of the Se-deficient mice increased by 0.2486 % after being infected with HAdV-14, indicating that the degree of lung inflammatory injury of the Se-deficient mice was higher than that of the normal mice, and Se might be involved in regulating HAdV-14 pneumonia (Figs. 6C and 7B). The increase of lung index in Se-deficient mice indicated that the mice infected with HAdV-14 developed pneumonia, which was manifested by inflammatory cell exudation and tissue inflammatory proliferation. HE staining was performed on the lung tissue sections of different groups of mice to observe the morphological changes and inflammatory responses of the lung tissue. As shown in Fig. 7C and D, compared with the control group, the mice in the virus group had a large amount of inflammatory cell exudation in the lung parenchyma, the alveolar tissue structure collapsed in different sizes, and a mass of tissues and epithelial cells proliferated in the lung. Pulmonary inflammation was improved after SeNPs@LNT treatment, manifested as reduced inflammatory hyperplasia of lung tissue and inflammatory cell exudation, and alveolar structure returned to normal. TUNEL-DAPI assay was performed on the lung tissue of different groups of mice to detect DNA fragmentation in the lung tissue. HAdV-14 infection might lead to DNA damage in the interstitial and nucleus of the lung tissue of Se-deficient mice. However, SeNPs@LNT effectively repaired DNA damage in mouse lungs induced by HAdV-14 infection (Fig. 7C). It was demonstrated that SeNPs@LNT alleviated lung tissue damage by inhibiting viral infection-mediated DNA damage.

There are many pathogenic mechanisms for the damage caused by virus infection. The inflammatory cytokine storm induced by pro-inflammatory cytokines makes the immune regulation disorder of the body is one of the most common mechanisms [57,58]. Immunohistochemical staining of mouse lung tissue showed that the protein expressions of T-NFκB and T-Stat3 were significantly increased in the lung tissue of Se-deficient mice infected with HAdV-14 (Fig. 7J). The NFκB-mediated signaling pathway is involved in the response of cells to external stimuli, and promotes the production of corresponding

cytokines to participate in the response. NFκB plays a key role in the process of cellular inflammatory response and immune response [59, 60]. The results showed that HAdV-14 infection as an external stimulus activated the NFκB signaling pathway. Immediately, we detected inflammatory cytokines in the serum of mice, and found that the levels of IL-8, IL-12p70, IL-17 A, IL-22, and TNF-β in the virus group increased, among which the levels of IL-8, TNF-β, and IL-22 were significantly increased. After SeNPs@LNT treatment, the expressions of T-NFκB and T-Stat3 proteins in lung tissue were down-regulated, while the levels of inflammatory cytokines in mouse serum recovered to lower levels (Fig. 7E–H). In the context of immune system disturbances, an excessive cellular immune response can lead to a storm of inflammatory cytokines and damage to host cells. We speculated that since the mice were in Se-deficient conditions, they might develop more severe adenovirus pneumonia after infection with HAdV-14. The virus acted as an exogenous stimulus to activate the production of inflammatory cytokines, and the excessive immune response caused the body damage. SeNPs@LNT treatment effectively supplemented the Se element in the systemic circulation of Se-deficient mice, inhibited the infection of HAdV-14 and down-regulated the NFκB signaling pathway. This was also consistent with previous research [61]. Thus, the level of inflammatory cytokines in the systemic circulation of mice was effectively reduced, and the excessive immune response mediated by inflammatory cytokine storm was avoided. After SeNPs@LNT treatment, the viral load in the lung tissue of Se-deficient mice was significantly reduced, further verifying the antiviral effect of SeNPs@LNT (Fig. 7I).

In order to explore the molecular biological mechanism of SeNPs@LNT curing Se-deficient mice, immunohistochemical staining experiments were performed on lung tissues of mice in different groups. The apoptosis signaling pathway mediated by DNA damage was explored by detecting the expression of T-PARP protein. The cell cycle signaling pathway mediated by mitochondrial function was explored by detecting the expression of Bcl-XL and Bcl-2 proteins. By detecting the expression of p-Akt (Ser473) and T-Erk1/2 proteins, the anti-apoptotic regulatory signaling pathway was explored. The results showed that the expression of the pro-apoptotic protein T-PARP was significantly increased in the virus group compared with the control group. Meanwhile, the expressions of p-Akt (Ser473) and T-Erk1/2 anti-apoptotic proteins were significantly down-regulated. Similar to the regulation of signaling pathways in the *in vitro* cell experiments, the expression of Bcl-xL and Bcl-2 proteins in the virus group decreased, inhibiting their anti-apoptotic activities, thereby mediating mitochondrial oxidative damage to induce apoptosis [62]. However, the virus + SeNPs@LNT group significantly inhibited the expression of the pro-apoptotic protein T-PARP, and at the same time up-regulated the expression of the anti-apoptotic proteins Bcl-xL, Bcl-2, p-Akt (Ser473) and T-Erk1/2 (Fig. 7J).

3.11. SeNPs@LNT increases Se content in lung tissue and converted it into a metabolic program of selenoenzymes in Se-deficient mice

In the *in vivo* models of Se-deficient mice, SeNPs@LNT was administered by gavage to ensure that the quantitative drug was taken up by the mice. In order to further investigate whether SeNPs@LNT could accumulate active ingredients such as Se elements into the target organs of HAdV-14 infection through the systemic circulation after entering into mice. The Se content in the lung tissue from mice in different groups was detected by ICP-MS. The results showed that compared with the mice of the control group, the Se content of the mice in the virus group was reduced to a certain extent, and the Se content of mice in the SeNPs@LNT group was increased. Surprisingly, the Se content of mice in the virus + SeNPs@LNT group was also higher than that in the control group and virus group (Fig. 8A). Meanwhile, SeNPs@LNT treatment could significantly up-regulate the Se content in serum of Se-deficient mice infected with HAdV-14 (Fig. 8B). We speculate that in the Se-deficient mouse model, SeNPs@LNT can not only supplement the Se

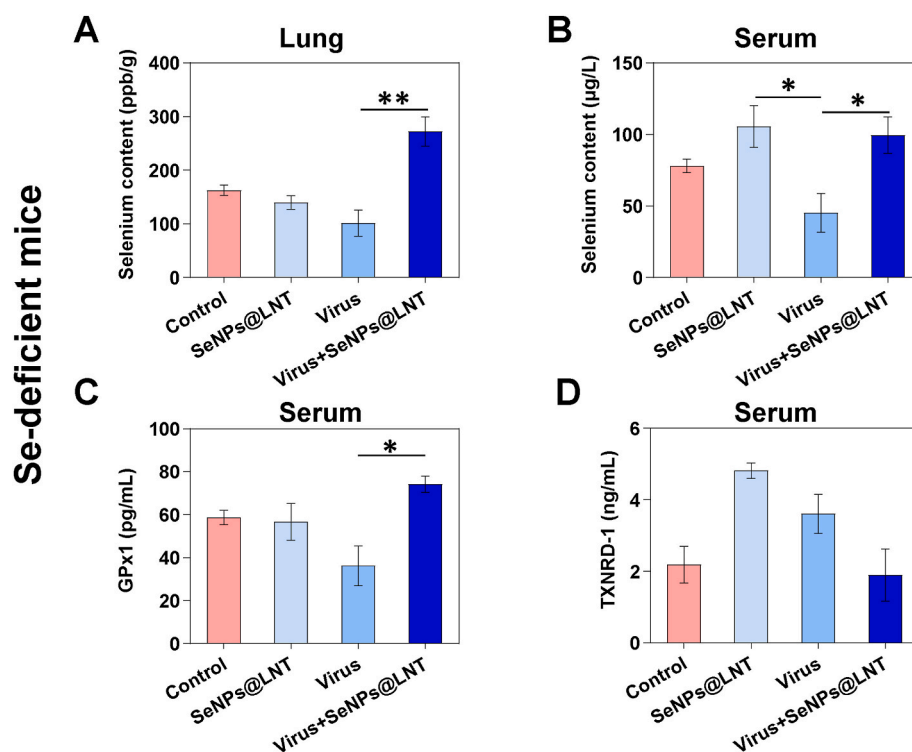


Fig. 8. SeNPs@LNT increases the Se content in lung tissue and serum of Se-deficient mice, and participates in the metabolic process of Se through selenoprotein. The level of Se content in (A) the lung tissue and (B) the serum of mice in different groups; (C) The level of GPx1 in the serum of mice in different groups; (D) The level of TXNRD-1 in the serum of mice in different groups. The therapeutic concentration of SeNPs@LNT was 0.2 mg Se/kg. Bars with different characters are statistically different at $P < 0.05$ (*) or $P < 0.01$ (**) level.

content at the site of HAdV-14 infection, but also upregulate the Se content in the systemic circulation, thereby effectively alleviating the Se-deficiency state in the whole body of mice.

Selenoproteins were key components in redox reactions, in which GPx played an important role in antioxidant defense. Previous studies have found that when Se was deficient, GPx1 would undergo significant changes, which were manifested in decline of enzyme activity, protein expression and mRNA level [63]. Some research had shown that Se was an essential component of the catalytic reaction of GPx1, which catalyzed glutathione to decompose peroxides in the body [64]. Most importantly, the occurrence and development of many diseases, especially viral infections and tumors, were related to ROS, and the activity of GPx1 decreased to varying degrees during the pathogenesis [65]. Therefore, SeNPs@LNT metabolites, including two important selenoenzymes, GPx1 and TXNRD-1, were detected by ELISA. By means of semi-quantitative detection, the results demonstrated that the level of GPx1 in the serum of the mice in the virus group decreased, while the level of GPx1 in the serum of the mice was significantly increased after SeNPs@LNT treatment (Fig. 8C). However, TXNRD-1 was down-regulated after SeNPs@LNT treatment compared to virus group (Fig. 8D). We speculated that SeNPs@LNT increased the content of Se in the lung tissue of mice after entering the systemic circulation, and further exhibited antioxidant and antiviral biological activities by converting into GPx1, which had a significant repair effect on the oxidative stress damage caused by HAdV-14. The experimental results supported the speculation that SeNPs@LNT increases the Se content at the infection site as well as in the systemic circulation, and further exhibited oxidative stress-regulating activity through conversion to GPx1.

4. Conclusions

In this study, we discovered and synthesized a kind of SeNPs@LNT nanoparticles with excellent bioactivity. SeNPs@LNT resists adenovirus

pneumonia by inhibition the oxidative stress response caused by HAdV-14 infection in mice. SeNPs@LNT reduced the damage caused by HAdV-14 infection by selenoprotein to inhibit the inflammatory cytokine storm in the serum of Se-deficient mice. By maintaining the stability of mitochondrial function, reducing the production of ROS, repairing DNA damage, reducing the production of progeny viruses, and inhibiting the signaling pathway of apoptosis, the infection of HAdV-14 is alleviated.

This study possesses the following advantages: (i) SeNPs@LNT has been validated in cell and animal models with the characteristics of low toxicity and excellent antiviral effect, which means potential development prospects; (ii) The experiments have proved that anti-oxidative reaction is one of the important directions of SeNPs@LNT in anti-HAdV-14 infection; (iii) SeNPs@LNT could effectively increase the Se content in the lungs and could up-regulate the GPx1 level in the systemic circulation, effectively alleviating the inflammatory cytokine storm mediated by HAdV-14 infection, proving the utilization of SeNPs@LNT in biology; (iv) The research and development of the anti-HAdV-14 therapeutic mechanism of SeNPs@LNT could help to fill the gap of adenovirus lacking specific therapeutic drugs. Thus, SeNPs@LNT might provide a small molecular Se-containing nanoparticles with effective anti-HAdV-14 virus properties.

Conflicts of interest

The authors report no conflicts of interest in this work.

5. Ethics approval and consent to participate

This project was approved by the Ethics Committee of Guangzhou Women and Children Medical Center (approval number: 2,017,021,803).

6. Data availability statement

The data that support the findings of this study are openly available.

CRedit authorship contribution statement

Yinghua Li: Writing – original draft, Methodology, Investigation, Funding acquisition, Conceptualization. **Ting Liu:** Writing – original draft, Methodology, Investigation. **Ruilin Zheng:** Writing – review & editing, Methodology, Investigation. **Jia Lai:** Methodology, Investigation. **Jingyao Su:** Writing – review & editing. **Jiali Li:** Writing – review & editing. **Bing Zhu:** Writing – review & editing, Supervision, Methodology. **Tianfeng Chen:** Writing – review & editing, Supervision, Funding acquisition, Conceptualization.

Declaration of competing interest

The authors declare that they have no known competing financial interests or personal relationships that could have appeared to influence the work reported in this paper.

Acknowledgements

This work was supported by the fund from the Open Project of Guangdong Key Laboratory of Marine Material (LMM2020-7), the technology planning projects of Guangzhou (202201020655 and 202102010202), the Guangdong Natural Science Foundation (2020A15110648), the Open Fund of Guangdong Provincial Key Laboratory of Functional Supramolecular Coordination Materials and Applications (2020A03), and the Guangzhou Medical University Students' Science and Technology Innovation Project (2023ekky009 and 02-408-2203-2079).

Appendix A. Supplementary data

Supplementary data to this article can be found online at <https://doi.org/10.1016/j.bioactmat.2024.04.034>.

References

- M.G. Ison, R.T. Hayden, Adenovirus, *Microbiol. Spectr.* 4 (2016) 1–14.
- Q. Ma, X. Tian, Z. Jiang, J. Huang, Q. Liu, X. Lu, Q. Luo, R. Zhou, Neutralizing epitopes mapping of human adenovirus type 14 hexon, *Vaccine* 33 (2015) 6659–6665.
- J.K. Louie, A.E. Kajon, M. Holodniy, L. Guardia-Labar, B. Lee, A.M. Petru, J. K. Hacker, D.P. Schnurr, Severe pneumonia due to adenovirus serotype 14: a new respiratory threat? *Clin. Infect. Dis.* 46 (2008) 421–425.
- D.H. Esposito, T.J. Gardner, E. Schneider, et al., Outbreak of pneumonia associated with emergent human adenovirus serotype 14—Southeast Alaska, 2008, *J. Infect. Dis.* 202 (2) (2010) 214–222.
- Q. Zhang, D. Seto, S. Zhao, L. Zhu, W. Zhao, C. Wan, Genome sequence of the first human adenovirus type 14 isolated in China, *J. Virol.* 86 (2012) 7019–7020.
- X. Tian, Y. Fan, C. Wang, Z. Liu, W. Liu, Y. Xu, C. Mo, A. You, X. Li, X. Rong, R. Zhou, Seroprevalence of neutralizing antibodies against six human adenovirus types indicates the low level of herd immunity in young children from Guangzhou, China, *Virology* 36 (2021) 373–381.
- A.M. Alcamo, M.S. Wolf, L.J. Alessi, H.J. Chong, M. Green, J.V. Williams, D. W. Simon, Successful use of cidofovir in an immunocompetent child with severe adenoviral sepsis, *Pediatrics* 145 (2020) e20191632.
- T. Lion, Adenovirus infections in immunocompetent and immunocompromised patients, *Clin. Microbiol. Rev.* 27 (2014) 441–462.
- P. Martínez-Aguado, A. Serna-Gallego, J.A. Marrugal-Lorenzo, I. Gómez-Marín, J. Sánchez-Céspedes, Ant adenovirus drug discovery: potential targets and evaluation methodologies, *Drug Discov. Today* 20 (2015) 1235–1242.
- M.J. Dodge, K.M. Macneil, T.M. Tessier, J.B. Weinberg, J.S. Mymryk, Emerging antiviral therapeutics for human adenovirus infection: recent developments and novel strategies, *Antivir. Res.* 188 (2021) 105034.
- K. Kosulin, E. Geiger, A. Vécsei, W.D. Huber, M. Rauch, E. Brenner, F. Wrba, K. Hammer, A. Innerhofer, U. Pötschger, A. Lawitschka, S. Matthes-Leodolter, G. Fritsch, T. Lion, Persistence and reactivation of human adenoviruses in the gastrointestinal tract, *Clin. Microbiol. Infect.* 22 (2016) 381.
- G.C. Fanning, F. Zoulim, J. Hou, A. Bertoletti, Therapeutic strategies for hepatitis B virus infection: towards a cure, *Nat. Rev. Drug Discov.* 18 (2019) 827–844.
- B.N. Williamson, F. Feldmann, B. Schwarz, K. Meade-White, D.P. Porter, J. Schulz, N. van Doremalen, I. Leighton, C.K. Yinda, L. Pérez-Pérez, A. Okumura, J. Lovaglio, P.W. Hanley, G. Saturday, C.M. Bosio, S. Anzick, K. Barbian, T. Cihlar, C. Martens, D.P. Scott, V.J. Munster, E. de Wit, Clinical benefit of remdesivir in rhesus macaques infected with SARS-cov-2, *Nature* 585 (2020) 273–276.
- A.P. Lea, H.M. Bryson, Cidofovir, *Drugs* 52 (1996) 225–230.
- G.N. Dailey, D. Ragoonan, A. Aboulhosn, Adenovirus infection and disease in recipients of hematopoietic cell transplantation, *Curr. Opin. Infect. Dis.* 32 (2019) 591–600.
- E. De Clercq, G. Li, Approved antiviral drugs over the past 50 years, *Clin. Microbiol. Rev.* 29 (2016) 695–747.
- J. Wang, H. Wang, X. Xia, P. Li, K. Wang, Inhibitory effect of sulfated lentinan and lentinan against tobacco mosaic virus (tmv) in tobacco seedlings, *Int. J. Biol. Macromol.* 61 (2013) 264–269.
- M. Jesenak, I. Urbancikova, P. Banovcin, Respiratory tract infections and the role of biologically active polysaccharides in their management and prevention, *Nutrients* 9 (2017) 779.
- G. Ren, L. Xu, T. Lu, J. Yin, Structural characterization and antiviral activity of lentinan from *Lentinula edodes* mycelia against infectious hematopoietic necrosis virus, *Int. J. Biol. Macromol.* 115 (2018) 1202–1210.
- B. Kaleta, A. Górski, R. Zagożdżon, M. Cieślak, J. Kaźmierczak-Barańska, B. Nawrot, M. Klimaszewska, E. Malinowska, S. Górka, J. Turlo, Selenium-containing polysaccharides from *Lentinula edodes*—biological activity, *Carbohydr. Polym.* 223 (2019) 115078.
- M.P. Rayman, Selenium and human health, *Lancet* 379 (2012) 1256–1268.
- X.D. Shi, Y.Q. Tian, J.L. Wu, S.Y. Wang, Synthesis, characterization, and biological activity of selenium nanoparticles conjugated with polysaccharides, *Crit. Rev. Food Sci. Nutr.* 61 (2021) 2225–2236.
- H. Yang, C. Liu, Y. Wu, M. Yuan, J. Huang, Y. Xia, Q. Ling, P.R. Hoffmann, Z. Huang, T. Chen, Atherosclerotic plaque-targeted nanotherapeutics ameliorates atherogenesis by blocking macrophage-driven inflammation, *Nano Today* 42 (2022) 101736.
- T. Liu, L. Xu, L. He, J. Zhao, Z. Zhang, Q. Chen, T. Chen, Selenium nanoparticles regulates selenoprotein to boost cytokine-induced killer cells-based cancer immunotherapy, *Nano Today* 35 (2020) 100971–100975.
- S. Liu, W. Wei, J. Wang, T. Chen, Theranostic applications of selenium nanomedicines against lung cancer, *J. Nanobiotechnol.* 21 (2023) 96.
- H. Lai, L. Xu, C. Liu, S. Shi, Y. Jiang, Y. Yu, B. Deng, T. Chen, Universal selenium nanoadjuvant with immunopotentiating and redox-shaping activities inducing high-quality immunity for SARS-cov-2 vaccine, *Signal Transduct. Targeted Ther.* 8 (2023) 88.
- G. Chen, F. Yang, S. Fan, H. Jin, K. Liao, X. Li, G.B. Liu, J. Liang, J. Zhang, J.F. Xu, J. Pi, Immunomodulatory roles of selenium nanoparticles: novel arts for potential immunotherapy strategy development, *Front. Immunol.* 13 (2022) 956181.
- J. Pi, L. Shen, E. Yang, H. Shen, D. Huang, R. Wang, C. Hu, H. Jin, H. Cai, J. Cai, G. Zeng, Z.W. Chen, Macrophage-targeted isoniazid-selenium nanoparticles promote antimicrobial immunity and synergize bactericidal destruction of tuberculosis bacilli, *Angew. Chem., Int. Ed. Engl.* 59 (2020) 3226–3234.
- J.J. Ojeda, M.L. Merroun, A.V. Tugarova, S. Lampis, A.A. Kamnev, P.H.E. Gardiner, Developments in the study and applications of bacterial transformations of selenium species, *Crit. Rev. Biotechnol.* 40 (2020) 1250–1264.
- S. Menon, S.K.S. Devi, R. Santhiya, S. Rajeshkumar, V.S. Kumar, Selenium nanoparticles: a potent chemotherapeutic agent and an elucidation of its mechanism, *Colloid Surf. B-Biointerfaces* 170 (2018) 280–292.
- J. Ouyang, B. Deng, B. Zou, Y. Li, Q. Bu, Y. Tian, M. Chen, W. Chen, N. Kong, T. Chen, W. Tao, Oral hydrogel microbeads-mediated in situ synthesis of selenoproteins for regulating intestinal immunity and microbiota, *J. Am. Chem. Soc.* 145 (2023) 12193–12205.
- C. Weiss, M. Carriere, L. Fusco, I. Capua, J.A. Regla-Nava, M. Pasquali, J.A. Scott, F. Vitale, M.A. Unal, C. Mattevi, D. Bedognetti, A. Merkoçi, E. Tasciotti, A. Yilmazer, Y. Gogotsi, F. Stellacci, L.G. Delogu, Toward nanotechnology-enabled approaches against the covid-19 pandemic, *ACS Nano* 14 (2020) 6383–6406.
- S. Mukherjee, P. Mazumder, M. Joshi, C. Joshi, S.V. Dalvi, M. Kumar, Biomedical application, drug delivery and metabolic pathway of antiviral nanotherapeutics for combating viral pandemic: a review, *Environ. Res.* 191 (2020) 110119.
- T. Yadavalli, D. Shukla, Role of metal and metal oxide nanoparticles as diagnostic and therapeutic tools for highly prevalent viral infections, *Nanomedicine* 13 (2016) 219–230.
- H. Wu, X. Li, W. Liu, T. Chen, Y. Li, W. Zheng, C.W. Man, M. Wong, K. Wong, Surface decoration of selenium nanoparticles by mushroom polysaccharides-protein complexes to achieve enhanced cellular uptake and antiproliferative activity, *J. Mater. Chem.* 22 (2012) 9602–9610.
- S. Liu, N. Li, H. Lai, L. Xu, Y. Zeng, X. Chen, H. Huang, T. Chen, J. Liu, J. Wang, Selenium nanoparticles enhance nk cell-mediated tumoricidal activity in malignant pleural effusion via the trxr1-il-18rap-pstat3 pathway, *Adv. Funct. Mater.* (2024) 2401264.
- B. Xie, D. Zeng, M. Yang, Z. Tang, L. He, T. Chen, Translational selenium nanoparticles to attenuate allergic dermatitis through nr2-keap1-driven activation of selenoproteins, *ACS Nano* 17 (2023) 14053–14068.
- Z. Song, W. Luo, H. Zheng, Y. Zeng, J. Wang, T. Chen, Translational nanotherapeutics reprograms immune microenvironment in malignant pleural effusion of lung adenocarcinoma, *Adv. Healthc. Mater.* 10 (2021) 2100149.
- M. Wang, R. Cao, L. Zhang, X. Yang, J. Liu, M. Xu, Z. Shi, Z. Hu, W. Zhong, G. Xiao, Remdesivir and chloroquine effectively inhibit the recently emerged novel coronavirus (2019-ncov) in vitro, *Cell Res.* 30 (2020) 269–271.

- [40] F. Liu, Y. Huang, Q. Wang, H. Shan, Construction of egfp-tagged senecavirus a for facilitating virus neutralization test and antiviral assay, *Viruses* 12 (2020) 283.
- [41] S. Takano, S. Shiimoto, K.Y. Inoue, K. Ino, H. Shiku, T. Matsue, Electrochemical approach for the development of a simple method for detecting cell apoptosis based on caspase-3 activity, *Anal. Chem.* 86 (2014) 4723–4728.
- [42] C. Wang, Y. Xia, S. Huo, D. Shou, Q. Mei, W. Tang, Y. Li, H. Liu, Y. Zhou, B. Zhu, Silencing of mef2d by sirna loaded selenium nanoparticles for ovarian cancer therapy, *Int. J. Nanomed.* 15 (2020) 9759–9770.
- [43] Y.C. Lin, C. Chipot, S. Scheuring, Annexin-v stabilizes membrane defects by inducing lipid phase transition, *Nat. Commun.* 11 (2020) 230.
- [44] N.D. Georgakopoulos, G. Wells, M. Campanella, The pharmacological regulation of cellular mitophagy, *Nat. Chem. Biol.* 13 (2017) 136–146.
- [45] Y. Li, Z. Lin, M. Guo, M. Zhao, Y. Xia, C. Wang, T. Xu, B. Zhu, Inhibition of h1n1 influenza virus-induced apoptosis by functionalized selenium nanoparticles with amantadine through ros-mediated akt signaling pathways, *Int. J. Nanomed.* 13 (2018) 2005–2016.
- [46] L. He, G. Huang, H. Liu, C. Sang, X. Liu, T. Chen, Highly bioactive zeolitic imidazolate framework-8-capped nanotherapeutics for efficient reversal of reperfusion-induced injury in ischemic stroke, *Sci. Adv.* 6 (2020) eaay9751.
- [47] B. Deng, X. He, D. Wang, Y. Wang, Y. Jiang, T. Chen, L. Xu, Designing selenium nanoadjuvant as universal agent for live-killed virus-based vaccine, *Small Methods* 7 (2023) e2300293.
- [48] Y. Li, D. Chen, J. Su, M. Chen, T. Chen, W. Jia, B. Zhu, Selenium-ruthenium complex blocks H1N1 influenza virus-induced cell damage by activating Gpx1/TrxR1, *Theranostics* 13 (2023) 1843–1859.
- [49] P.J. de Pablo, M.C. San, Seeing and touching adenovirus: complementary approaches for understanding assembly and disassembly of a complex virion, *Curr. Opin. Virol.* 52 (2021) 112–122.
- [50] M. Schieber, N.S. Chandel, Ros function in redox signaling and oxidative stress, *Curr. Biol.* 24 (2014) R453–R462.
- [51] R. Singh, A. Letai, K. Sarosiek, Regulation of apoptosis in health and disease: the balancing act of bcl-2 family proteins, *Nat. Rev. Mol. Cell Biol.* 20 (2019) 175–193.
- [52] Z. Wyzewski, W. Switlik, M.B. Mielcarska, K.P. Gregorczyk-Zboroch, The role of bcl-xl protein in viral infections, *Int. J. Mol. Sci.* 22 (2021) 1956.
- [53] C. Liu, K. Chen, H. Wang, Y. Zhang, X. Duan, Y. Xue, H. He, Y. Huang, Z. Chen, H. Ren, H. Wang, C. Zeng, Gastrin attenuates renal ischemia/reperfusion injury by a pi3k/akt/bad-mediated anti-apoptosis signaling, *Front. Pharmacol.* 11 (2020) 540479.
- [54] N. Pandey, B.E. Black, Rapid detection and signaling of dna damage by parp-1, *Trends Biochem. Sci.* 46 (2021) 744–757.
- [55] L.Y. Su, Y.X. Shi, M.R. Yan, Y. Xi, X.L. Su, Anticancer bioactive peptides suppress human colorectal tumor cell growth and induce apoptosis via modulating the parp-p53-mcl-1 signaling pathway, *Acta Pharmacol. Sin.* 36 (2015) 1514–1519.
- [56] W. Wang, C. Zeng, Y. Feng, F. Zhou, F. Liao, Y. Liu, S. Feng, X. Wang, The size-dependent effects of silica nanoparticles on endothelial cell apoptosis through activating the p53-caspase pathway, *Environ. Pollut.* 233 (2018) 218–225.
- [57] R. Zheng, Y. Li, D. Chen, J. Su, N. Han, H. Chen, Z. Ning, M. Xiao, M. Zhao, B. Zhu, Changes of host immunity mediated by ifn-gamma (+) cd8(+) t cells in children with adenovirus pneumonia in different severity of illness, *Viruses* 13 (2021) 2384.
- [58] D.C. Fajgenbaum, C.H. June, Cytokine storm, *N. Engl. J. Med.* 383 (2020) 2255–2273.
- [59] F. Wandrer, C.S. Falk, K. John, B. Skawran, M.P. Manns, K. Schulze-Osthoff, H. Bantel, Interferon-mediated cytokine induction determines sustained virus control in chronic hepatitis c virus infection, *J. Infect. Dis.* 213 (2016) 746–754.
- [60] W.P. Chong, M.J. Mattapallil, K. Raychaudhuri, S.J. Bing, S. Wu, Y. Zhong, W. Wang, Z. Chen, P.B. Silver, Y. Jittayasothorn, C.C. Chan, J. Chen, R. Horai, R. Caspi, The cytokine il-17a limits th17 pathogenicity via a negative feedback loop driven by autocrine induction of il-24, *Immunity* 53 (2020) 384–397.
- [61] S.K. Nettleford, K.S. Prabhu, Selenium and selenoproteins in gut inflammation—a review, *Antioxidants* 7 (2018) 36.
- [62] K. Ma, Z. Zhang, R. Chang, H. Cheng, C. Mu, T. Zhao, L. Chen, C. Zhang, Q. Luo, J. Lin, Y. Zhu, Q. Chen, Dynamic pgam5 multimers dephosphorylate bcl-xl or fundc1 to regulate mitochondrial and cellular fate, *Cell Death Differ.* 27 (2020) 1036–1051.
- [63] P. Zhang, X. Guan, M. Yang, L. Zeng, C. Liu, Roles and potential mechanisms of selenium in countering thyrotoxicity of dehp, *Sci. Total Environ.* 619–620 (2018) 732–739.
- [64] D. Song, Y. Cheng, X. Li, F. Wang, Z. Lu, X. Xiao, Y. Wang, Biogenic nanoselenium particles effectively attenuate oxidative stress-induced intestinal epithelial barrier injury by activating the nrf 2 antioxidant pathway, *ACS Appl. Mater. Interfaces* 9 (2017) 14724–14740.
- [65] Q. Sun, Y. Yang, Z. Wang, X. Yang, Y. Gao, Y. Zhao, W. Ge, J. Liu, X. Xu, W. Guan, D. Weng, S. Wang, J. Wang, J. Zhang, Per 1 interaction with gpx1 regulates metabolic homeostasis under oxidative stress, *Redox Biol.* 37 (2020) 101694.